

Article

Metamorphism and P-T Evolution of High-Pressure Granulites from the Fuping Complex, North China Craton

Zijing Zhang¹, Changqing Zheng^{1,2,*}, Chenyue Liang^{1,2} , M. Santosh^{3,4}, Junjie Hao⁵, Lishuai Dong⁵, Jianjun Hou⁵, Feifei Hou⁵ and Meihui Li¹

¹ College of Earth Sciences, Jilin University, Changchun 130061, China; zijing21@mails.jlu.edu.cn (Z.Z.); chenyueliang@jlu.edu.cn (C.L.); meihui21@mails.jlu.edu.cn (M.L.)

² Key Laboratory of Mineral Resources Evaluation in Northeast Asia, Ministry of Natural Resources, Changchun 130061, China

³ School of Earth Sciences and Resources, China University of Geoscience Beijing, 29 Xueyuan Road, Beijing 100083, China; santosh@cugb.edu.cn

⁴ Department of Earth Sciences, University of Adelaide, Adelaide, SA 5005, Australia

⁵ No. 9 Geological Team of Hebei Bureau of Geology and Mineral Resources Exploration, Xingtai 054000, China; 111haojunjie@163.com (J.H.); donglishuaidzjd@163.com (L.D.); houjianjun1122@163.com (J.H.); houfeifeidzjd@163.com (F.H.)

* Correspondence: zhengchangqing@jlu.edu.cn

Abstract: Granulite facies rocks provide important keys to evaluating collisional metamorphism in orogenic belts. The mafic granulites of Baoding in the Fuping Complex of the North China Craton occur within the Trans-North China Orogen (TNCO), a major Paleoproterozoic collisional orogen. Here, we present results from detailed investigations on newly discovered garnet pyroxenite, garnet two-pyroxene granulite, and garnet-bearing-plagioclase amphibolite using petrographic, mineralogical, geochemical, and zircon U-Pb dating methods. Our results show that the Fuping Complex metamorphic evolution in this study evolved in four stages: prograde (M_1), high-pressure granulite facies (M_2), granulite facies (M_3), and retrograde (M_4) stages. The mineral assemblage of the prograde stage (M_1) consists of Amp + Pl + Q within garnet cores. The mineral assemblage of high-pressure granulite facies at the peak stage (M_2) consists of Gt + Cpx + Pl + Q \pm Amp, forming the garnet pyroxenite. The granulite facies stage M_3 is characterized by the occurrence of orthopyroxene, with a mineral assemblage of Gt + Cpx + Opx + Amp + Pl + Q. The early retrograde stage M_{4-1} includes clinopyroxenes scattered inside amphiboles, following the breakdown of garnet and clinopyroxene. The mineral assemblage of this stage comprises Amp + Pl + Q + Ilm \pm Cpx. Later, in the late retrograde stage M_{4-2} , the composition of amphiboles changed to actinolite, and epidote and chlorite started to appear in the matrix. Traditional geothermobarometry yielded P-T conditions of 700~706 °C and 6.0~6.2 kbar for prograde stage M_1 , 854~920 °C and 13.0~13.8 kbar for high-pressure granulite facies stage M_2 , 912~939 °C and 8.1~9.9 kbar for M_3 , 661~784 °C and 3.1~4.4 kbar for M_{4-1} , and 637~638 °C, 1.1~1.3 kbar for M_{4-2} , along a clockwise P-T path with a nearly isothermal decompression (ITD) and slight heating. Zircon LA-ICP-MS U-Pb dating constrains the timing of the high-pressure granulite facies metamorphic event to be between 1.83 and 1.86 Ga. Geochemical features suggest that the protoliths of the high-pressure granulites may have formed in an island arc environment within a convergent margin setting. Together with results from previous studies, our data suggest that the ~1.85 Ga metamorphic age recorded in the Fuping Complex represents a regional metamorphism in the TNCO, associated with the subduction–collision and assembly of the Eastern and Western Blocks of the NCC.

Keywords: Fuping Complex; high-pressure granulite; clockwise P-T path; Trans-North China Orogen



Citation: Zhang, Z.; Zheng, C.; Liang, C.; Santosh, M.; Hao, J.; Dong, L.; Hou, J.; Hou, F.; Li, M. Metamorphism and P-T Evolution of High-Pressure Granulites from the Fuping Complex, North China Craton. *Minerals* **2024**, *14*, 138. <https://doi.org/10.3390/min14020138>

Academic Editor: Bernhard Schulz

Received: 21 November 2023

Revised: 19 January 2024

Accepted: 22 January 2024

Published: 26 January 2024



Copyright: © 2024 by the authors. Licensee MDPI, Basel, Switzerland. This article is an open access article distributed under the terms and conditions of the Creative Commons Attribution (CC BY) license (<https://creativecommons.org/licenses/by/4.0/>).

1. Introduction

The North China Craton (NCC) is one of the oldest cratonic blocks in the world, preserving records of Archean to late Palaeoproterozoic crustal evolution, cratonization,

and related geodynamic history that are important in understanding continental growth in the early Earth [1–7]. Based on differences in geochronology, rock assemblages, and P-T paths [8,9], the Precambrian basement within the NCC has been subdivided into several tectonic units, including the Western Block (WB), Eastern Block (EB), and the intervening Trans-North China Orogen (TNCO; [6,7]). The north–south trending TNCO comprises several basement terranes including Zanhuang, Fuping, Wutai, Hengshan, Huai’an, Xuanhua, Northern Hebei, and Chengde Complexes. The linear structural belts [10,11], retrograde eclogites and high-pressure granulites [12], clockwise P-T paths involving near-isothermal decompression, and metamorphic ages of 1.96–1.80 Ga [13,14] define the TNCO as a collisional orogenic belt between the EB and WB. Subduction and collision during continental assembly usually produce high-pressure metamorphism, therefore, understanding the P-T evolution of high-pressure granulites can provide crucial constraints on the evolution of lower crust involved in continental collision processes [15]. High-pressure granulites are mostly found in the northern TNCO and southern Jiao-Liao-Ji Belt of the Paleoproterozoic, also exposed in the south Yinshan Block, midwestern Khondalite Belt, and East Hebei, and usually display a Grt + Cpx + Pl + Q assemblage in mafic rocks and Grt + Ky + K-feldspar assemblage in metapelites and felsic rocks [16,17]. High-pressure mafic granulite in the TNCO was reported from the Huai’an–Manjinggou–Xuanhua–Xiwangshan region and afterwards from Harley and Cheng [18–20]. Along the Fuping–North Hengshan–Huai’an–Xuanhua–Chengde sector, these rocks define a northeast-oriented high-pressure granulite belt.

The Fuping Complex, located in the central TNCO, exposes granulite to lower-amphibolite-facies metapelitic rocks in the supra-crustal sequence, such as pelitic granulite, sillimanite-bearing gneiss, garnet–biotite gneiss, and garnet-bearing schist [21–23]. This suggests that compared to grt-ky-kfeld matrix rocks in other parts of the TNCO, it experienced lower P. Previous studies on the Fuping granulites focused on the peak conditions of the granulite facies [24,25]. Liu [24] noted that the mafic granulite of the Fuping Complex experienced a peak stage with P-T conditions of 751–833 °C/8.5–10.8 kbar and displayed a clockwise P-T path, suggesting early thickening to late tectonic uplift. Zhao et al. [25] reported P-T conditions from peak mineral assemblage of mafic granulite as 840–940 °C/8.7–9.7 kbar and defined a clockwise ITD-type P-T path. The metamorphism is dated as ~1.8 Ga, suggesting that the Fuping Complex underwent crustal thickening, tectonic denudation (uplift), and final cooling. However, Wei et al. [26] suggested that the mineral assemblages and textures of granulites from the Fuping Complex are similar to the high-pressure granulite of North Hengshan, indicating a similar metamorphic evolutionary process.

The Neoproterozoic metamorphic strata in the Fuping Complex mainly belong to the Yuanfang Formation of the Fuping Group, where the grade of metamorphism ranges from high-amphibolite facies to granulite facies. This study focuses on the high-pressure mafic granulites in the Yuanfang Group. We report detailed results from our field investigations, petrographic and mineralogical analyses, and geochronological studies. We reconstruct the metamorphic evolutionary history, and combined with the information from other segments of the TNCO, our study provides insights into the Precambrian HP metamorphic evolution of the TNCO.

2. Geologic Setting

The study area is located in Liangang Town of Yixian, north of Baoding City in Hebei Province. It is part of the northeastern Fuping Complex in the TNCO, close to the Eastern Block of the NCC (Figure 1). The stratigraphy in the area is widely exposed, ranging from the Neoproterozoic to the Cenozoic, with the stratigraphy of each generation being visible. The stratigraphy in the study area generally spreads in the northeast direction, from northwest to southeast, from old to new exposure. It can be divided into three main parts: Neoproterozoic metamorphic crystalline basement, Meso-Neo Proterozoic and Paleozoic sedimentary strata, and Cenozoic sediments. The Yuanfang Formation of the Fuping Group

occurs mainly in the form of remnant blocks within the Neoproterozoic metamorphic plutons, which are unconformably overlain by the Paleoproterozoic sedimentary cover.

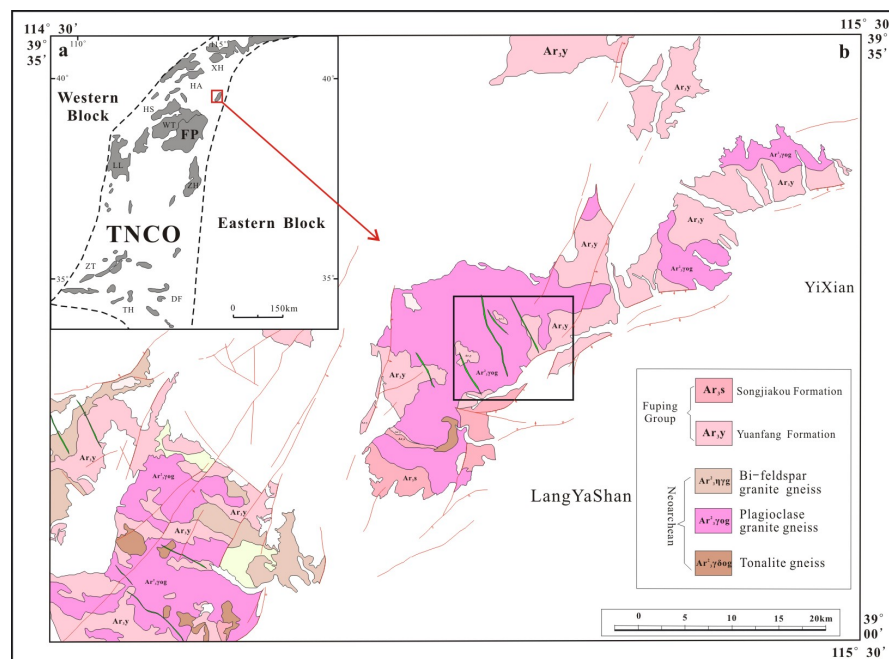


Figure 1. (a) Tectonic subdivision of the North China Craton (modified after [6]). (b) Geological map of the region. The portion in the center box is enlarged for Figure 2.

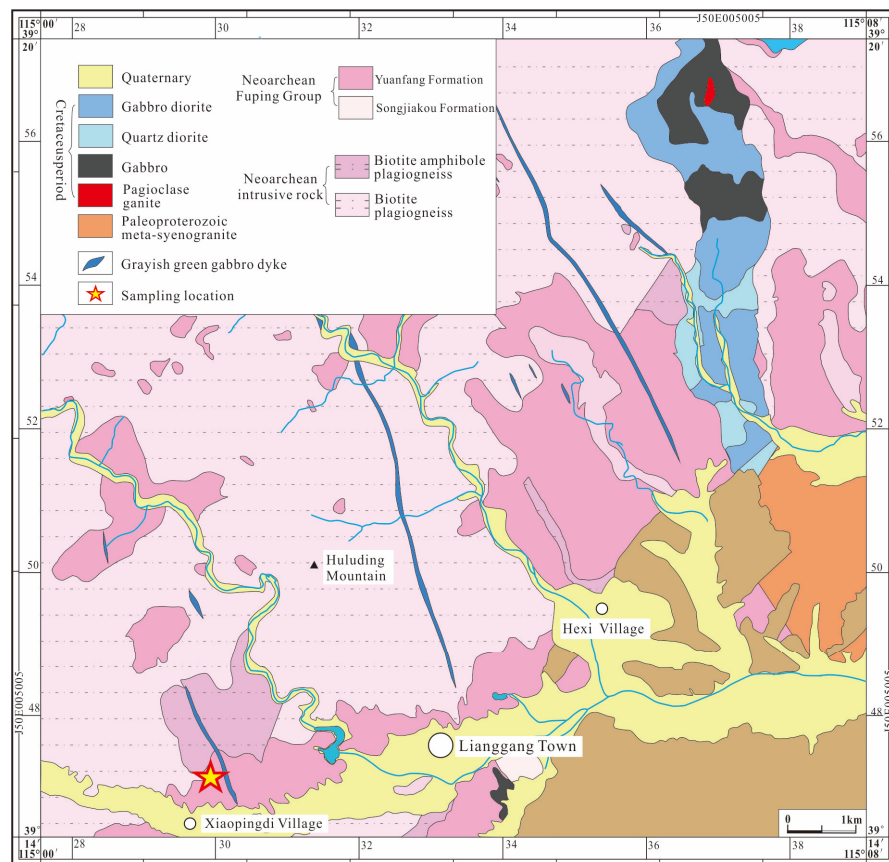


Figure 2. Geological map of the study area with sampling locations of representative samples.

The Yuanfang Formation is the oldest stratigraphic unit in the Taihangshan subregion (West Hebei) and was mapped at 1:50,000 scale by the Xiaojue-Mengjiazhuang district survey of the Hebei District Survey Institute's Ninth Branch in 1995. The rock assemblage is dominated by biotite–plagioclase gneisses and amphibolite gneisses, interspersed with amphibolite and minor leptynite. Locally, hornblende-bearing magnetite quartzite, garnet two-pyroxene granulite, and garnet pyroxenite also occur. The contact between the Yuanfang Formation and the Neoproterozoic metamorphic rocks is largely conformable with the gneissosity (Figure 2).

3. Petrography

The studied samples were collected from the northern part of Xiaopingdi Village, Liangang Town of Yixian, Baoding City, Hebei Province. The sampling locations are shown in Figure 2. The high-pressure granulites in the study area are mainly garnet pyroxenite, that underwent retrograde metamorphism to garnet two-pyroxene granulite and garnet-bearing-plagioclase amphibolite.

3.1. Garnet Pyroxenite

The main minerals in garnet pyroxenite (Figure 3a,b) include garnet (20~35%) + clinopyroxene (25~35%) + plagioclase (10~15%) + amphibole (10~25%) + quartz (5~8%), the secondary minerals are rutile, ilmenite, titanite, apatite, and magnetite. The samples show a porphyroblastic texture with amphibole + plagioclase (\pm clinopyroxene) coronae surrounding garnet porphyroblasts (Figure 3e,g,h). Garnet porphyroblasts, up to 2.5 mm in diameter, contain inclusions of quartz, amphibole, and plagioclase in the core (Figure 3c). Some garnets are fine-grained without inclusions, displaying a grain size of 0.25 to 0.75 mm, and are of the same generation as the coarse type (Figure 3d). The matrix of the samples mainly comprises subhedral clinopyroxene, plagioclase, amphibole, and quartz with minor ilmenite (Figure 3d). Relict clinopyroxenes in the matrix coexist adjacent to amphibole and plagioclase (Figure 3f), and some of the clinopyroxenes retrograde into amphiboles (Figure 3h). Amphibole and plagioclase mainly occur in several of these structural forms.

3.2. Garnet Two-Pyroxene Granulite

The main minerals found in garnet two-pyroxene granulite (Figure 4a,b) include garnet (20~25%) + amphibole (15~30%) + clinopyroxene (7~15%) + orthopyroxene (5~10%) + plagioclase (10~15%) + quartz (5%), and the secondary minerals are rutile, actinolite, epidote, chlorite, ilmenite, and magnetite. The rock has a porphyroblastic texture with diverse crystals of garnet and a matrix of clinopyroxene, orthopyroxene, plagioclase, and amphibole. The garnets in this rock sample display distinct cleavage, and the mineral assemblage of the prograde stage is indiscernible (Figure 4c). Relict clinopyroxene and orthopyroxene grains coexist in equilibrium with plagioclase in the matrix, and particles contain hornblende exsolution within them. Some of the rims of clinopyroxene and orthopyroxene are converted and transformed into amphiboles (Figure 4c–e). Amphiboles can be broadly divided into two associations: hypidiomorphic larger grains in the matrix (Figure 4g) and a “white-eye socket” structure with plagioclase around the rims of the garnets (Figure 4c). Plagioclase can also be broadly categorized into two types: matrix plagioclase (Figure 4h), partly in equilibrium with clinopyroxene and orthopyroxene, and the form of the “white-eye socket” structure. Epidote, chlorite, and actinolite are visible in some samples (Figure 4f,h), indicating retrograde metamorphism under high-greenschist to low-amphibolite facies.

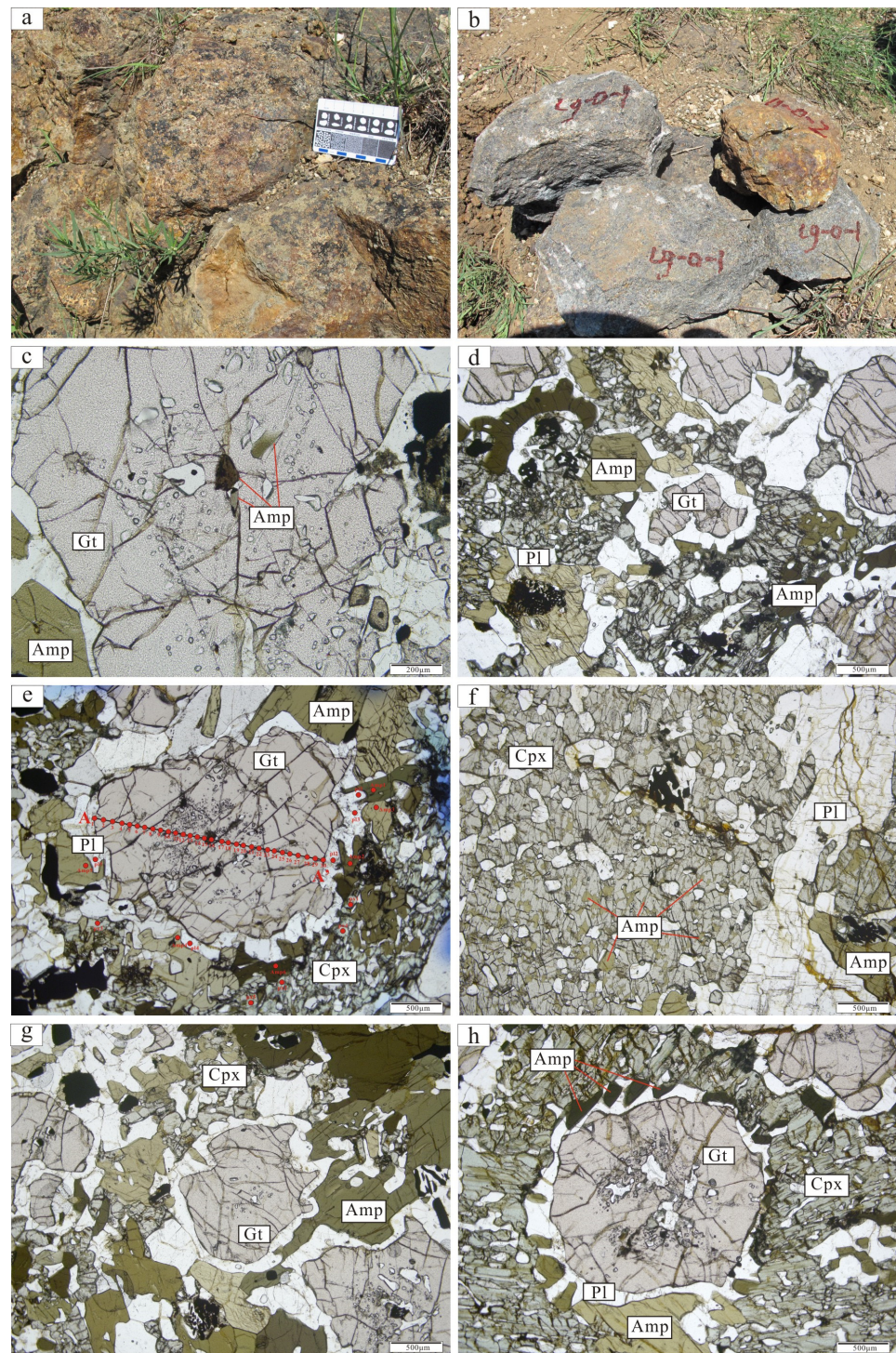


Figure 3. Representative macro- and microscopic photographs of petrographic features of garnet pyroxenite. (a,b) Macroscopic features; (c) Plagioclase and amphibole inclusions within garnet core; (d) The fine grains garnet and matrix minerals; (e) The amphibole + plagioclase (\pm clinopyroxene) coronae surrounding garnet porphyroblasts; (f) Relict clinopyroxenes; (g) The amphibole and plagioclase corona texture; (h) The clinopyroxenes retrograde into amphiboles. Pl: plagioclase; Gt: garnet; Cpx: clinopyroxene; Amp: amphibole.

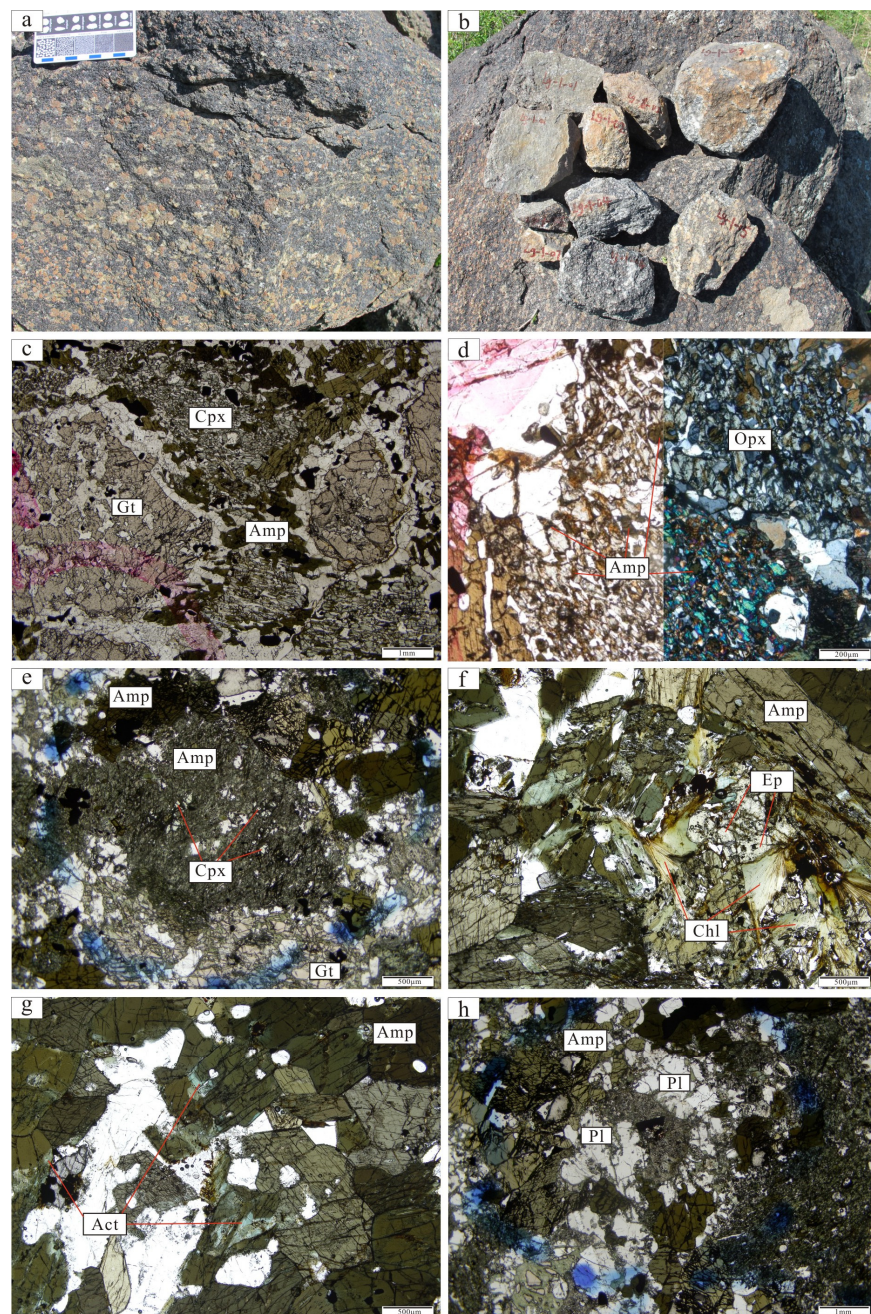


Figure 4. Representative macro- and microscopic photographs of petrographic features of garnet two-pyroxene granulite. (a,b) Macroscopic features; (c) The garnet with amphibole and plagioclase surrounding; (d) Relic clinopyroxene and orthopyroxene coexist in equilibrium with plagioclase in the matrix; (e) Some of the rims of clinopyroxene and orthopyroxene are converted to amphiboles; (f) The appearance of epidote and chlorite; (g) The actinolite; (h) The matrix plagioclase. Pl: plagioclase; Gt: garnet; Cpx: clinopyroxene; Opx: orthopyroxene; Amp: amphibole; Act: actinolite; Ep: epidote; Chl: chlorite.

3.3. Garnet-Bearing-Plagioclase Amphibolite

The garnet-bearing-plagioclase amphibolite (Figure 5a,b) contains garnet (5~10%) + amphibole (50~65%) + plagioclase (10~15%) + quartz (5~7%), and ilmenite, with accessory titanite and apatite. The fine-grained garnet in the sample could be the residue of the large porphyroblast garnets, which were partly consumed (Figure 5c,d). The hypidiomorphic amphiboles in the matrix may have formed during the retrograde stage (Figure 5e). The

plagioclase distributed in the matrix, and some in contact with the retrograde amphibole, may be the remnants from during the peak stage, while the others formed in the “white-eye socket” structure surrounding the garnets (Figure 5f) during the retrograde stage.

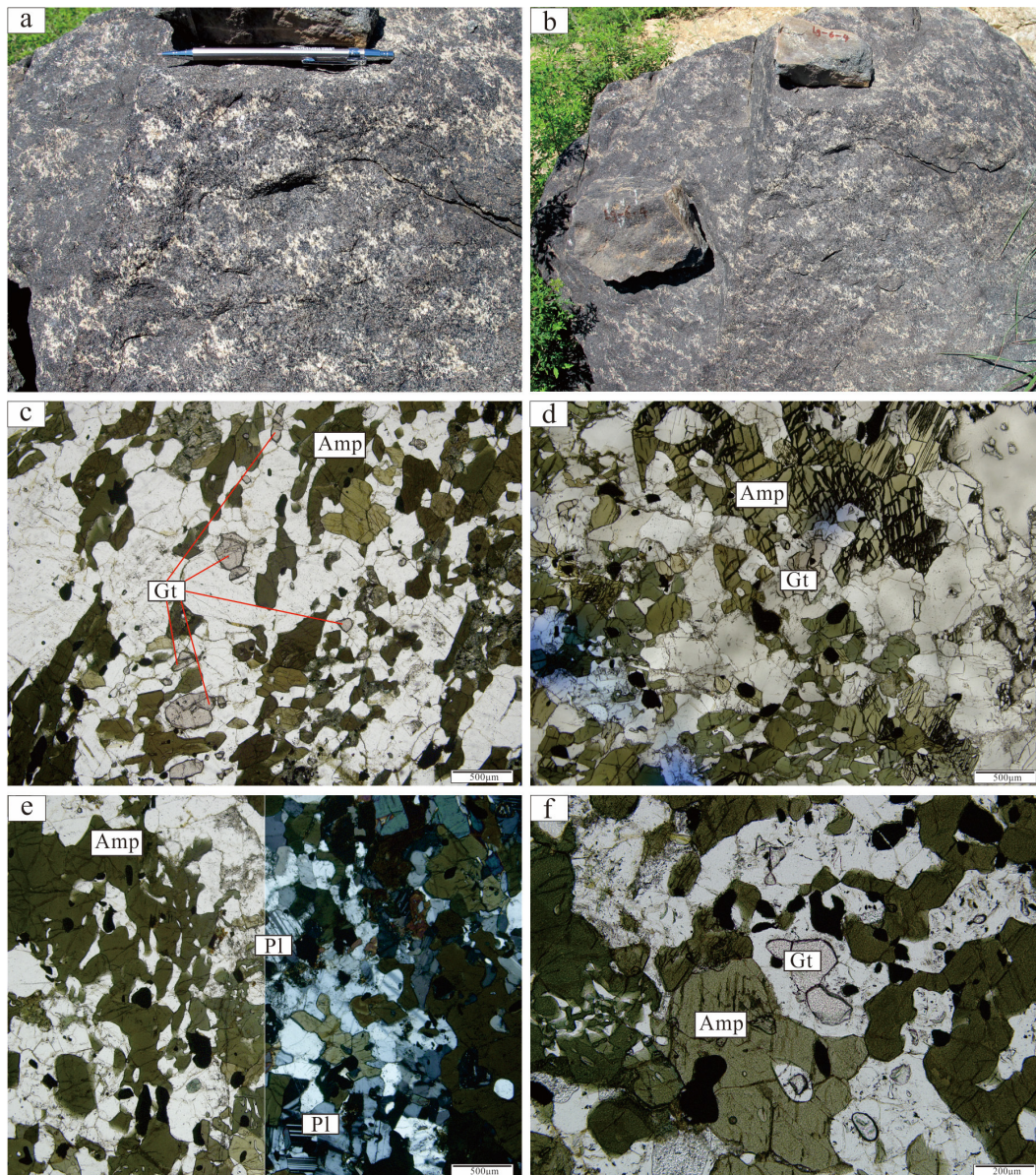


Figure 5. Representative macro- and microscopic photographs of petrographic features of garnet-bearing-plagioclase amphibolite. (a,b) Macroscopic features; (c,d) The remnants finegrain garnet; (e) The hypidiomorphic amphibole with larger size in the matrix; (f) The “white-eye socket” structure. Pl: plagioclase; Gt: garnet; Amp: amphibole.

Based on the reaction structures and mineral assemblages of the studied samples and combined with information from previous studies, we initially delineate the metamorphic stages. Different rock types record different stages of the same metamorphic evolution.

Garnet pyroxenite records three stages: the mineral association in the prograde stage as Amp + Pl inclusions within garnet cores; the peak mineral assemblage is Gt + Cpx + Pl + Q ± Amp; the mineral assemblage of the retrograde stage is the Amp + Pl coronal around the garnet rim.

Garnet two-pyroxene granulite records two stages: the peak stage mineral assemblage of this type of rock is Gt + Cpx + Opx + Amp + Pl + Q; early retrograde stage mineral

assemblages are the Amp + Pl coronal around the garnet, the late retrograde stage is characterized by the occurrence of Amp + Ep + Chl.

Garnet-bearing-plagioclase amphibolite only records the mineral assemblage of amphibole and plagioclase at the retrograde stage.

In summary, our integration of the metamorphic stages recorded in different rock types allows us to infer that the high-pressure metamorphism evolution of the study area is divided into four stages: prograde stage (M_1), high-pressure granulite facies stage (M_2), granulite facies stage (M_3), and retrograde stage (M_4).

- (1) The prograde stage M_1 assemblage consists of Gt-c + Amp + Pl + Q.
- (2) At the high-pressure granulite facies stage M_2 , the mineral assemblage of high-pressure granulite facies is composed of the garnet mantle, clinopyroxene core, and matrix plagioclase: Gt + Cpx + Pl + Q \pm Amp.
- (3) The granulite facies stage (M_3) is characterized by the occurrence of orthopyroxene, the mineral assemblage of this stage is composed of the garnet rim and matrix minerals: Gt + Cpx + Opx + Amp + Pl + Q.
- (4) The retrograde stage was characterized mainly by the amphibole + plagioclase corona texture around the garnet and the partial replacement of clinopyroxene by amphibole: early in the retrograde stage M_{4-1} , after the metamorphic crystallization, garnet and clinopyroxene were partly broken down, and the rims of residual clinopyroxene and orthopyroxene are converted to amphiboles. In some samples, the decomposition of garnet was almost complete, the assemblage of this stage consists of Amp + Pl + Q + Ilm \pm Cpx; late in the retrograde stage M_{4-2} , the epidote and chlorite appeared in the matrix, the assemblage of this stage consists of Amp + Ep + Chl.

4. Geochemistry

Whole-rock analysis of major and trace elements and rare earth elements was performed at the laboratory of the Ninth Geological Brigade of Hebei Provincial Bureau of Geology and Mineral Resources Exploration and Development. The analysis of major elements was carried out by an X-ray fluorescence spectrometer (XRF), while trace elements and rare earth elements were determined by an ICAP-Q inductively coupled plasma mass spectrometer, and the analytical techniques followed those in the “Methods of chemical analysis of silicate rocks—Part 30: Determination of 44 elemental” GB/T 14506.30-2010 [27].

In this study, 11 samples were selected for whole-rock analysis, including 4 garnet pyroxenites, 4 garnet two-pyroxene granulites, and 3 garnet-bearing-plagioclase amphibolites. The major, trace, and rare earth element data of all analyzed samples are given in Supplementary Tables S1 and S2.

4.1. Major Elements

The garnet pyroxenite contains $\text{SiO}_2 = 48.58\sim 51.26$ wt.%, $\text{TiO}_2 = 1.26\sim 1.87$ wt.%, $\text{Al}_2\text{O}_3 = 11.06\sim 14.32$ wt.%, $\text{MgO} = 4.91\sim 6.25$ wt.%, $\text{CaO} = 9.07\sim 11.45$ wt.%, and $\text{P}_2\text{O}_5 = 0.24\sim 0.38$ wt.%. $\text{K}_2\text{O}/\text{Na}_2\text{O}$ ratios range from 0.13 to 0.28, with K_2O content being much lower than Na_2O 's. The $\text{Mg}^\#$ ($100 \times \text{MgO}/(\text{FeO}^{\text{T}} + \text{MgO})$) ranges mostly from 36.50 to 39.07, which is lower than the range of primary basaltic magma ($\text{Mg}^\# = 68\sim 75$), indicating that the protolith magma of garnet pyroxenite underwent a lower degree of magmatic differentiation [28].

The garnet two-pyroxene granulite contains $\text{SiO}_2 = 48.68\sim 52.30$ wt.%, $\text{TiO}_2 = 1.44\sim 1.83$ wt.%, $\text{Al}_2\text{O}_3 = 12.59\sim 14.00$ wt.%, $\text{MgO} = 5.22\sim 6.91$ wt.%, $\text{CaO} = 8.22\sim 9.09$ wt.%, $\text{P}_2\text{O}_5 = 0.21\sim 0.27$ wt.%. The Na_2O contents are higher than that of K_2O , with mass fractions ranging from 1.26 to 1.86 wt.% and 0.38 to 0.67 wt.%, respectively. The range of $\text{Mg}^\#$ is from 38.57 to 46.67, which might be related to the segregation and crystallization of mafic minerals in the magma [28].

The garnet-bearing-plagioclase amphibolite contains $\text{SiO}_2 = 51.31\sim 52.42$ wt.%, $\text{TiO}_2 = 1.38\sim 1.48$ wt.%, $\text{Al}_2\text{O}_3 = 12.80\sim 13.13$ wt.%, $\text{MgO} = 5.38\sim 5.66$ wt.%, $\text{CaO} = 9.02\sim 9.12$ wt.%, $\text{P}_2\text{O}_5 = 0.20\sim 0.24$ wt.%. The contents of Na_2O are higher than that of K_2O , the mass frac-

The garnet pyroxenite has slight negative anomalies of Th, P, Zr, and Y and strong negative anomalies of Rb, Nb, Sr, and Ti. The mass fractions of compatible elements (Cr, Ni, and Sc) are 65.2×10^{-6} – 120.0×10^{-6} , 33.7×10^{-6} – 71.9×10^{-6} , 32.7×10^{-6} – 44.2×10^{-6} , respectively; the mass fractions of high-field-strength elements Zr, Hf, and Th do not vary much in the samples.

The garnet two-pyroxene granulite has strong positive anomalies of U, Nd, and Dy and strong negative anomalies of Ba, Nb, Sr, and Zr. The mass fractions of compatible elements (Cr, Ni, and Sc) range from 52.1×10^{-6} – 142.0×10^{-6} , 45.5×10^{-6} – 73.5×10^{-6} , 34.2×10^{-6} – 40.6×10^{-6} , respectively, and those of the high-field-strength elements (Zr, Hf, Nb, Ta, Y, Th, and U) are relatively high, except for Th and U, that have high mass fractions of individual samples, while the elemental mass fractions from the rest of the samples were not much changed.

The garnet-bearing-plagioclase amphibolites have strong positive anomalies of U, Nd, and Dy and strong negative anomalies of Nb, Sr, Zr, and Ti. The mass fractions of compatible elements (Cr, Ni, and Sc) range from 71.4×10^{-6} – 88.8×10^{-6} , 39.3×10^{-6} – 52.8×10^{-6} , 34.3×10^{-6} – 41.5×10^{-6} , respectively, and the mass fractions of high-field-strength elements Hf and Y do not vary much in the samples.

The Ni and Cr contents of all analyzed samples are lower than those of the primary magma (Ni = 250×10^{-6} , Cr = 300×10^{-6}), indicating that the protoliths have undergone crystallization and separation rather than forming directly from the original magma. The garnet pyroxenite and its retrograde metamorphic products show an overall enrichment in U and depletion in Nb, Sr, and Ti, according to the primitive mantle-normalized trace elements spider diagram (Figure 6c). The depletion in Ti may be related to the segregated crystallization of ilmenite. The depletion in Sr may also be caused by the segregated crystallization of plagioclase under low-pressure conditions. However, the negative Eu anomalies, which are the most significant indicator of segregated crystallization of plagioclase, are weaker, making the depletion of Sr more likely to be related to the source area. Except for the samples of garnet-bearing-plagioclase amphibolite, Ba and Zr also exhibit relative depletions.

4.4. Protolith Characteristics and Tectonic Setting

Shaw [33] proposed that the X-function can be used to differentiate the protolith types of metamorphic rocks and avoid the influence of metasomatism by excluding more reactive elements such as K, Na, and Si. The discriminant function is:

$$X = -2.69\lg\text{Cr} - 3.18\lg\text{V} - 1.25\lg\text{Ni} + 10.57\lg\text{Co} + 7.73\lg\text{Sc} + 7.5\lg\text{Sr} - 1.95\lg\text{Ba} - 1.99\lg\text{Zr} - 19.58.$$

For metamorphic rocks, a positive X-value implies that the protolith is magmatic, whereas a negative X-value indicates that the protolith is a sediment. The high-pressure granulites and their retrograde products typically have positive X-values ranging from 5.91 to 6.61, 2.21 to 3.34, and 2.92 to 4.03, respectively. This indicates that the protoliths of these rocks are all igneous. Some of the garnet pyroxenites show negative X-values, which are attributed to strong negative anomalies in Sr. Combined with trace elements research, it is inferred that the low Sr content in these samples is more likely to be related to the source area.

The TAS diagram shows that the protoliths of garnet pyroxenite, garnet two-pyroxene granulite, and garnet-bearing-plagioclase amphibolite are basalt and basaltic andesite (Figure 6a). The SiO_2 - $\text{K}_2\text{O} + \text{Na}_2\text{O}$ diagram developed by Irvine and Baragar [14] for basal rocks (Figure 7a) indicates that the data points of the high-pressure granulite and its retrograde products fall in the subalkaline series, which encompasses both the calc-alkaline and tholeiitic series. Yin [34] pointed out that the Y-Zr diagram (Figure 7b) can determine whether the igneous rocks are tholeiitic or calc-alkaline series, and after mapping the data points, it is clear that the high-pressure granulite and retrograde products all belong to the tholeiitic series.

To determine the tectonic environment of the protolith formation, the linear discriminant analysis function using major elements proposed by Verma [35] was used (Figure 8). The plots show an island arc basalt (IAB) affinity. Among trace elements, La, Nb, and Th are relatively stable and minimally affected by late seawater alteration and metamorphism [36]. Here, we use the La/Nb-La and Th/Yb-Nb/Th tectonic environment discrimination diagrams (Figure 7c,d) [36] to trace the source area characteristics of the basalt. This approach is basically unaffected by partial melting and crystallization processes. Most of the data points fall within the island arc basalt (Figure 7a), suggesting that the fluids from the subducted slab interacted with the mantle wedge, leading to the partial melting and the formation of the island arc magma. At the same time, the adjacent oceanic lithospheric mantle may have experienced partial melting, giving rise to magma with EMORB affinities (Figure 7d). In summary, the protoliths of mafic granulite consist of basalt and basaltic andesite, with their primary magma belonging to the tholeiitic series, which were produced in the island arc environment of a convergent plate margin.

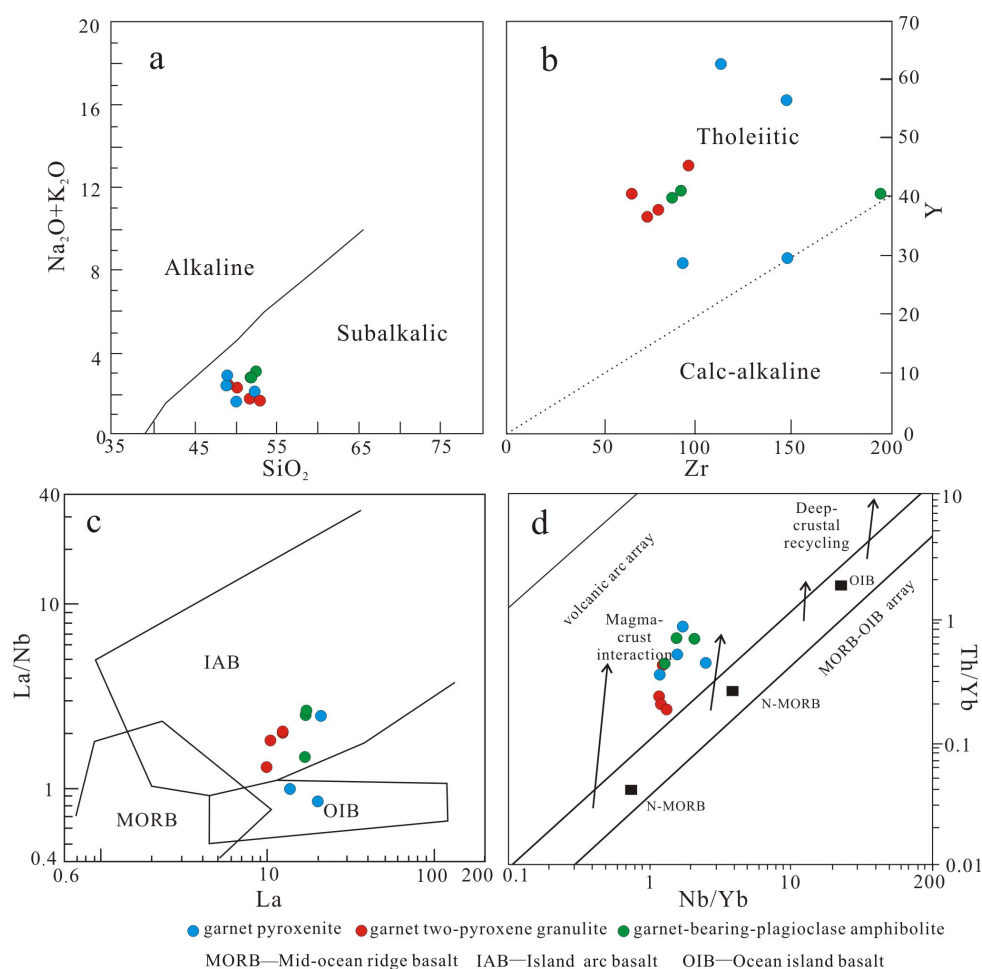


Figure 7. (a) $\text{SiO}_2\text{-K}_2\text{O} + \text{Na}_2\text{O}$ diagram [37]; (b) Y-Zr diagram [38]; (c) La/Nb-La diagrams; (d) Th/Yb-Nb/Yb [39].

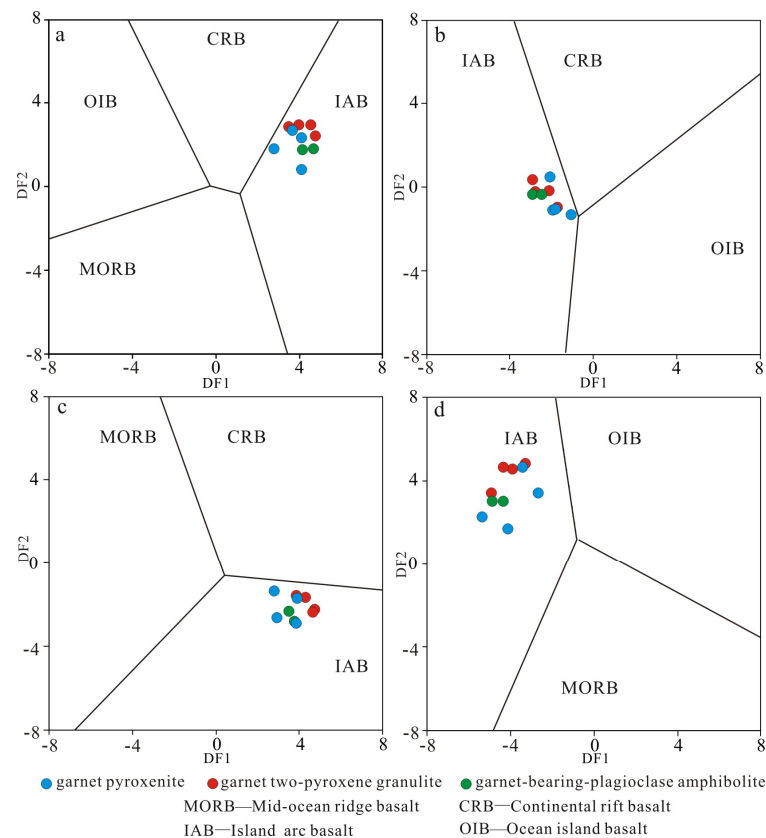


Figure 8. Tectonic discriminant diagrams of high-pressure granulites (after [35]).

5. Mineral Chemistry

Mineral compositions were determined using a JEOL JXA-8230 electron probe microanalyzer ((JEOL Ltd., Akishima, Tokyo, Japan)) at the College of Earth Science, Jilin University, Key Laboratory of Mineral Resources Evaluation of Northeast Asia, Ministry of Land and Resources, Changchun, China. Operation conditions involved a 15 kV acceleration voltage, a 10 nA beam current, and a beam diameter set to 1 μm for all minerals. Fifty-three minerals of the company SPI in the United States were used for standard calibrations. The calculation of mineral end components used AXE_2007 and the GCDkit programs.

Based on petrographic observations, electron microprobe analysis was performed on the samples that show metamorphic reactions and different generations of minerals. The analyzed minerals include garnet, clinopyroxene, orthopyroxene, amphibole, and plagioclase, and the chemical compositions of each mineral are described as follows.

5.1. Garnet

The results of the garnet analyses are listed in Supplementary Table S3. The composition types of garnet in garnet pyroxenite are almandine ($X_{\text{Alm}} = 0.53\text{--}0.60$), grossular ($X_{\text{Grs}} = 0.22\text{--}0.31$), pyrope ($X_{\text{Prp}} = 0.14\text{--}0.17$), and a small amount of spessartine ($X_{\text{Sps}} = 0.01\text{--}0.02$). X_{Fe} in garnets varies between 0.77 and 0.80. A compositional profile along the A-A' line (Figure 3c) was performed on the large porphyroblast garnet in representative sample Lg-0-01, and the chemical compositions of the profile are identified in Figure 9a. As seen in Figure 9a., the garnet exhibits obvious growth zoning with an increase in X_{Grs} (2.08~31.07) and a decrease in X_{Alm} (55.41~53.36) from the core to the mantle while the compositions of X_{Prp} are relatively constant. Typically, Ca in garnet is positively correlated with pressure, while the Fe/Mg ratio is negatively correlated with temperature [40]. The growth zoning in the garnet suggests that most garnet core compositions indicate the prograde stage, and from the prograde to the peak stage there is an increase in temperature and pressure. From the mantle to the rim, the compositional

characteristics of garnet, in general, show a significant increase in X_{Alm} and X_{Prp} and a significant decrease in X_{Grs} , indicating that in the retrograde stage there is a decrease in temperature and pressure [41]. In addition, the garnet rim exhibits diffusion zoning with obvious negative correlation variation of X_{Alm} , X_{Grs} , and X_{Prp} from the inside to the outside. The increase in X_{Alm} and the decrease in X_{Prp} suggest the existence of Fe-Mg interchange between garnet and the minerals in the matrix (clinopyroxene or amphibole), while the decrease in X_{Grs} causes the formation of plagioclase corona during the retrograde stage. The weak variation of X_{Sps} from the core to the mantle in garnet is because when the temperature increases, the competition between divergent crystallization and diffusion would result in the Mn elements homogenizing then demonstrating the flat zoning pattern of garnet [42]. Numerous studies have found that in high-grade metamorphic rocks, the Mn zoning of garnet shows a gradual flattening distribution characteristic with a gradual increase in metamorphic grade [34,43,44]. Some fine grains of garnet were also analyzed, and the compositions are similar to the garnet rim in large porphyroblast, indicating they may be the residual part of the large porphyroblast after decomposition from the core along the fissure.

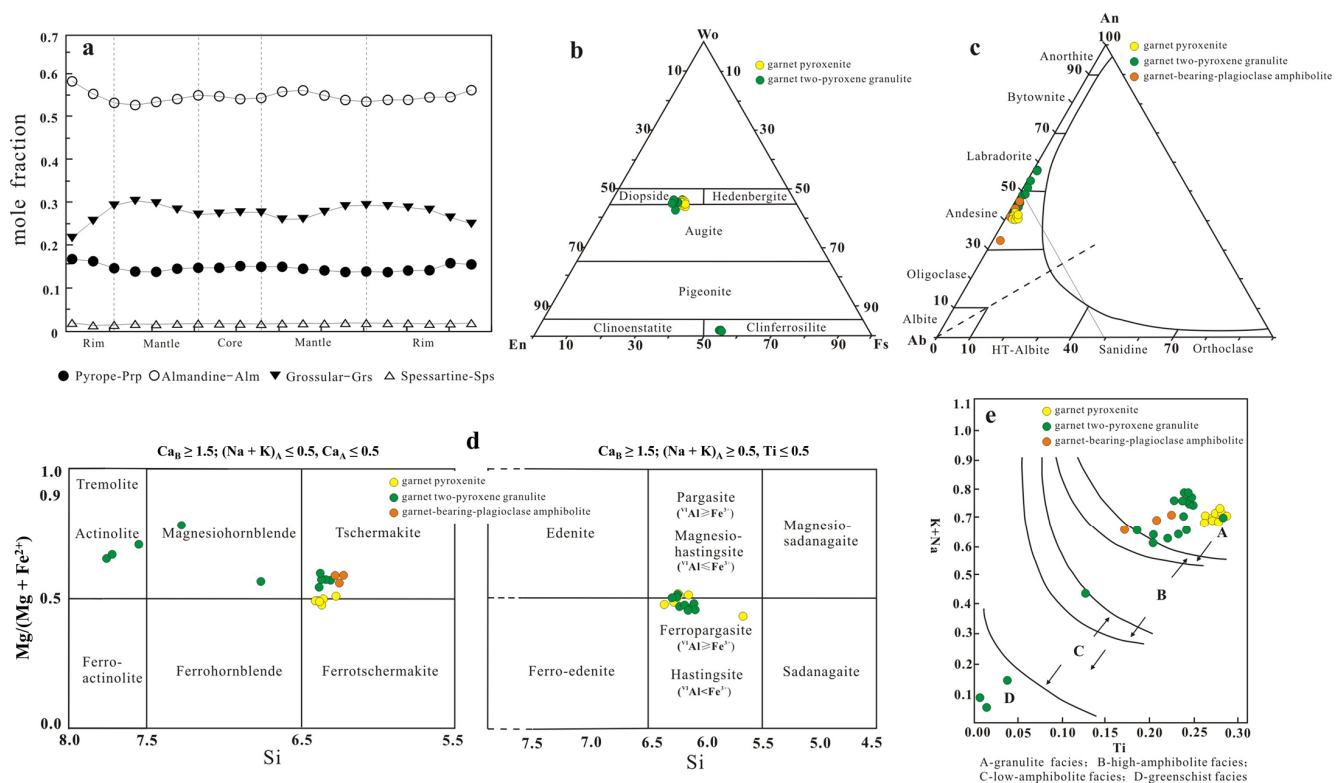


Figure 9. (a) Zoning profile of X_{Alm} , X_{Prp} , X_{Grs} , and X_{Sps} defined accordingly across garnet in garnet pyroxenite sample; (b) En-Wo-Fs classification diagram of pyroxene (after [45]); (c) Or-Ab-An compositional diagram of plagioclases; (d) Si-Mg/(Mg + Fe²⁺) classification diagram of hornblendes (after [45]); (e) Ti-(Na + K) composition relation diagram of hornblendes (after [46]).

The garnets in the garnet two-pyroxene granulite samples are mostly relict, with poorly characterized rim zones, and contain mainly almandine ($X_{Alm} = 0.55\sim 0.58$), grossular ($X_{Grs} = 0.19\sim 0.30$), and pyrope ($X_{Prp} = 0.12\sim 0.20$), with a small amount of spessartine ($X_{Sps} = 0.01\sim 0.04$). The X_{Fe} in garnets varies between 0.74 and 0.83. The reason for the wide range of garnet compositions may be the reaction of garnet with the inclusion of minerals or the presence of cracks in the garnet resulting in compositional changes [47].

The fine-grained garnet in the garnet-bearing-plagioclase amphibolite is distributed sporadically. Its compositional analysis resulted in high X_{Alm} (0.54~0.58) and low X_{Sps} (0.05~0.06) and X_{Grs} (0.19~0.25), with consistent X_{Prp} (0.15~0.17). Compared to the composi-

tion of garnet pyroxenite, the content of X_{Sps} is slightly higher, while X_{Alm} is lower. Studies on garnet composition have shown that the Mn element content decreases with the increase in rock formation temperature [25,48,49], indicating that garnet-bearing-plagioclase amphibolite should form in the retrograde stage.

5.2. Pyroxene

The results of the clinopyroxene and orthopyroxene analyses are listed in Supplementary Table S4. The clinopyroxenes in garnet pyroxenite exhibit similar chemical compositions, with $\text{SiO}_2 = 50.47\sim 52.58\%$, $\text{Al}_2\text{O}_3 = 1.65\sim 2.08\%$, $\text{Na}_2\text{O} = 0.34\sim 0.41\%$, $X_{\text{Mg}} = 0.60\sim 0.65$, $\text{Wo} = 0.43\sim 0.46$, $\text{En} = 0.33\sim 0.35$, $\text{Fs} = 0.20\sim 0.23$. They consist mainly of augite and diopside and are the products during the high-pressure granulite facies stage. The clinopyroxenes in garnet two-pyroxene granulite are strongly altered, its rim retrogrades into amphibole, and they are distributed only as a relic form in the amphibole core, with $\text{SiO}_2 = 50.22\sim 52.14\%$, $\text{Al}_2\text{O}_3 = 1.46\sim 2.18\%$, $\text{Na}_2\text{O} = 0.31\sim 0.40\%$, $\text{Wo} = 0.44\sim 0.46$, $\text{En} = 0.33\sim 0.36$, $\text{Fs} = 0.18\sim 0.22$, $X_{\text{Mg}} = 0.61\sim 0.73$, and their compositions are diopside and augite. The clinopyroxenes in this sample are affected by the retrograde metamorphism, thus having a higher En component and a lower Fs component (Figure 9b).

According to Anovitz [50], in the context of the same chemical composition, the degree of metamorphic pressure plays a decisive role in the Al_2O_3 content of clinopyroxene in mafic high-pressure granulites. The higher the pressure, the higher the Al_2O_3 content, and conversely, the lower the pressure, the lower the Al_2O_3 content. The analysis of clinopyroxene in garnet pyroxenite and garnet two-pyroxene granulite indicates that the Al_2O_3 in the clinopyroxene core is higher than that in the rim, suggesting that the pressure of the clinopyroxene core in high-pressure granulite is greater than that in the mantle and rim. Therefore, it can be concluded that retrograde metamorphism mainly affects the rim component [51], and the information about peak metamorphic pressure recorded in the core can be preserved.

Orthopyroxene occurs only in the granulite facies stage of garnet two-pyroxene granulite samples. The chemical composition of orthopyroxene grains in the matrix as well as the discrete grains shows homogeneity, suggesting equilibrium [52]. The MgO, FeO, and Al_2O_3 contents of orthopyroxene in the samples vary from 15.098 to 15.366, 31.858 to 32.306, 0.723 to 0.867, respectively. The CaO contents ranged from 0.38 to 0.47. The X_{Mg} varied from 0.45~0.46. According to the Morimoto et al. [29] classification, the mineral has a composition of clinoferrosilite (Figure 9b).

5.3. Amphibole

The results of the amphibole analysis are presented in Supplementary Table S5. The garnet pyroxenite has three types of amphibole. The amphibole inclusions in garnet core belong to the prograde metamorphism stage, with a component of MgO = 6.76~6.93%, FeO = 17.74~18.24%, $X_{\text{Mg}} = 0.40\sim 0.43$, $\text{Fe}^{3+} = 0.10\sim 0.21$, $\text{Al}^{\text{VI}} = 0.70\sim 0.80$ and belonging to ferropargasite (Figure 9d). The second type of blastohypidiomorphic amphibole occurs in the matrix during the retrograde stage and has two distribution forms. One type is located in the interior and rims of clinopyroxene, with MgO = 8.34~8.42%, FeO = 18.68~18.79%, $X_{\text{Mg}} = 0.49\sim 0.50$, and the components are ferrotschermakite, tschermakite, magnesiohastingsite, and hastingsite (Figure 9d), while the other surrounds the garnet in a “white-eye socket” structure, with a composition of MgO = 8.19~8.45%, FeO = 18.16~19.15%, $X_{\text{Mg}} = 0.47\sim 0.50$, and the components are ferrotschermakite, magnesiohastingsite, and hastingsite (Figure 9d). The third type of amphibole is formed through the metamorphic reaction of clinopyroxene, distributed in the peak clinopyroxene, and has unclear boundary, with MgO content of 8.38~8.67%, FeO = 18.53~18.80%, $X_{\text{Mg}} = 0.49\sim 0.51$, and the components are ferrotschermakite, magnesiohastingsite, and hastingsite (Figure 9d). All types of amphiboles above belong to granulite facies (Figure 9e), especially the inclusion of amphibole in garnet, indicating that the metamorphic degree of prograde stage may have reached the granulite facies.

The amphiboles in the garnet two-pyroxene granulite are of two types. One amphibole is hypidiomorphic with a larger size and located in the matrix, as well as forming a “white-eye socket” structure around the garnet, with the composition of MgO = 8.2~9.97%, FeO = 16.72~19.94%, $X_{Mg} = 0.43\sim 0.59$, and the components are tschermakite, magnesiohastingsite, ferropargasite, and hastingsite (Figure 9d), indicating the metamorphism degree of the high-amphibolite facies to granulite facies (Figure 9e). The other amphibole shows allotriomorphic granoblastic texture with relict clinopyroxene inside, and this kind of amphibole may have formed from the transformation of clinopyroxene. In the transition phase, the components are MgO = 10.77~14.24%, FeO = 14.07~16.08%, $X_{Mg} = 0.56\sim 0.71$, and the components are actinolite and magnesiohornblende (Figure 9d). The degree of metamorphism belongs to the upper greenschist to lower amphibolite facies (Figure 9e), indicating that the P-T condition of the late retrograde stage is equivalent to the low-amphibolite facies.

The amphiboles in garnet-bearing-plagioclase amphibolite are distributed hypidiomorphic corona in the matrix, partially surrounding the residual fine-grained garnet, with the composition of MgO = 9.12~9.37%, FeO = 17.57~18.13%, $X_{Mg} = 0.56\sim 0.59$. Their components are tschermakite (Figure 9d), and the metamorphism degree is equivalent to the granulite facies (Figure 9e).

In summary, the metamorphism degree of amphibole in high-pressure granite samples corresponds mainly to the granulite facies (average $X_{Mg} = 0.52$), followed by retrogression to the low-amphibolite facies (average $X_{Mg} = 0.62$) and high -greenschist facies (average $X_{Mg} = 0.71$). Therefore, the amphiboles are more Mg-rich in the retrograde metamorphic stage compared to the peak stage during the process of metamorphism.

5.4. Plagioclase

The results of the plagioclase analysis are listed in Supplementary Table S6. In the garnet pyroxenite, plagioclase occurs in two types: one developed during the retrograde stage, forming the coronal structure around the garnet rims, whereas the other coexists with clinopyroxene in the peak high-pressure granulite facies and is present within the matrix. Both the plagioclase in the corona ($X_{An} = 0.40\sim 0.43$) and the plagioclase which coexists with clinopyroxene ($X_{An} = 0.42\sim 0.44$) are andesine (Figure 9c). The CaO content of the plagioclase corona (8.36) is similar to that of the plagioclase situated within the clinopyroxene (8.66). Both types of plagioclase exhibit low K_2O content in the range of 0.335 to 0.493.

The plagioclase in the garnet two-pyroxene granulite occurs in two forms: the first one forms the “white-eye socket” structure surrounding garnet with $An = 0.39\sim 0.54$, while the other plagioclases coexist with clinopyroxene, orthopyroxene, and garnet in the matrix, representing the peak granulite stage mineral assemblage, with $An = 0.39\sim 0.65$. Both types of plagioclases are andesine and labradorite (Figure 9c), with the plagioclases in the matrix having higher CaO content (10.10). The K_2O content of plagioclases in the samples is low, ranging from 0.129 to 0.434.

The plagioclase in the garnet-bearing-plagioclase amphibolite is hypidiomorphic within the matrix, and the CaO content ranges from 6.85% to 9.49%, with Na_2O content ranging from 5.89% to 7.40%, $Ab = 52.19\sim 64.63\%$, and $X_{An} = 0.33\sim 0.46$, and it is identified as andesine (Figure 9c).

During the evolution of high-pressure granulite, Fe-rich garnets formed in the prograde stage. The Fe concentration of garnet falls and the Ca content rises as temperature and pressure rise. Among the minerals encased by garnet during this process are ferropargasite, plagioclase, and clinopyroxene. The inclusions within garnet can be thought of as the mineral assemblage of the prograde stage because the core component of well-crystallized garnet porphyroblast struggles to react with the environment [16,53]. The garnet component and the clinopyroxene and plagioclase in the matrix make up the majority of the mineral assemblage during the peak stage. The matrix clinopyroxenes are affected by the late-stage retrograde metamorphism, which causes the rim's Al_2O_3 content to be lower

than the core. The composition of the clinopyroxene rim is primarily affected by retrograde metamorphism, therefore the peak pressure information from the core is retained.

In the retrograde stage, the garnet rim shows a decrease in Ca and Mg content as temperature and pressure drop. This process results in the formation of the typical “white-eye socket” structure, consisting of amphibole and plagioclase. At the same time, the Fe content decreases and Mg content increases in clinopyroxene, along with the appearance of orthopyroxene, while ilmenite is formed through Fe released from amphibole. As a result of retrograde metamorphism, the Mg content of amphibole increases, and the amphibole gradually changes to magnesiohornblende and actinolite.

6. Metamorphic Evolution and P-T Path

Based on petrographic, geochemical, and mineral chemistry studies (Figure 10a), the evolution of high-pressure granulite facies metamorphism in Yixian is inferred to have occurred in four stages, including the prograde stage (M₁), the peak high-pressure granulite facies stage (M₂), the granulite facies stage (M₃), and the retrograde stage (M₄). Based on the paragenetic association of metamorphic minerals in each evolutionary stage, the P-T conditions of each metamorphic stage were calculated, mostly using a Grt-Cpx geothermometer [54], Grt-Cpx-Pl-Q geothermobarometry [55], Grt-Opx geothermometer [56], Grt-Opx geothermobarometry [57], Grt-Opx-Pl-Q geothermobarometry [58], Hbl geothermometer [59], and Hbl-Pl geothermobarometry [60] (Table 1).

Table 1. The estimated temperature and pressure conditions of high-pressure granulites.

Rock Type	Metamorphic Stage	Mineral Combinations	Metamorphosis Reaction	Thermobarometry	T (°C)	P (kbar)
Garnet pyroxenite	M ₁	Gt-c + Amp + Pl + Q		Hbl T	700~706	6.0~6.2
	M ₂	Gt + Cpx + Pl ± Amp + Q	Amp + Pl + Q → Gt + Cpx + Pl	Grt-Cpx T Grt-Cpx-Pl-Q PT	854~920	13.0~13.8
	M ₄₋₁	Amp + Pl + Q + Mag ± Cpx	Gt + Cpx + Q + H ₂ O → Amp + Pl + Mag	Hbl T Hbl-Pl PT	682~754	3.9~4.2
Garnet two-pyroxene granulite	M ₃	Gt + Cpx + Opx + Amp + Pl + Q	Gt + Cpx + Pl → Gt + Cpx + Opx + Pl Gt + Cpx + Q → Gt + Amp + Pl	Grt-Opx T Grt-Opx PT Grt-Opx-Pl-Q PT	912~939	8.1~9.9
	M ₄₋₁	Amp + Pl + Q + Mag ± Cpx	Gt + Cpx + Q + H ₂ O → Amp + Pl + Mag		661~784	3.1~4.4
	M ₄₋₂	Amp + Ep + Chl	Amp → Amp + Ep + Chl	Hbl T Hbl-Pl PT	637~638	1.1~1.3
Garnet-bearing-plagioclase amphibolite	M ₄₋₁	Amp + Pl + Q + Mag ± Cpx	Gt + Cpx + Q + H ₂ O → Amp + Pl + Mag		722~772	4.1~4.3

The garnet pyroxenite preserves the prograde, peak high-pressure granulite facies, and early retrograde stage of Yixian high-pressure granulite metamorphism. The mineral assemblage of the prograde metamorphic stage (M₁) is Amp₁ + Pl₁ + Q inclusions in the garnet core, and the estimated P-T conditions were T = 700~706 °C, P = 6.0~6.2 kbar, corresponding to the granulite facies. The mineral assemblage of the peak high-pressure granulite facies stage (M₂) is garnet porphyroblast with a relict clinopyroxene core part and plagioclase in the matrix: Gt + Cpx + Pl₂ + Q ± Amp. The possible metamorphic reactions in this stage are Amp₁ + Pl₁ → Gt + Pl₂, Amp₁ + Pl₁ + Q → Gt + Cpx + Pl₂ (Figure 10(b₁,b₂)). Based on the high-CaO component of garnet mantle, high-Al₂O₃ and -X_{Mg} component of clinopyroxene core, and low-An content in plagioclase, the P-T conditions of the peak stage are estimated to be T = 854~920 °C and P = 13.0~13.8 kbar, which are

equivalent to the high-pressure granulite facies. The mineral assemblage of the early retrograde stage (M_{4-1}) is $\text{Amp}_2 + \text{Pl}_3 + \text{Q} + \text{Mag} \pm \text{Cpx}$, and the possible metamorphic reaction is $\text{Gt} + \text{Cpx} + \text{Q} + \text{H}_2\text{O} \rightarrow \text{Amp}_2 + \text{Pl}_3 + \text{Mag}$ (Figure 10(b₃)). Based on the reaction rim component of amphibole and plagioclase around garnet, the P-T conditions are estimated at $T = 682\sim 754\text{ }^\circ\text{C}$, $P = 3.9\sim 4.2\text{ kbar}$, which correspond to the upper amphibolite to granulite facies.

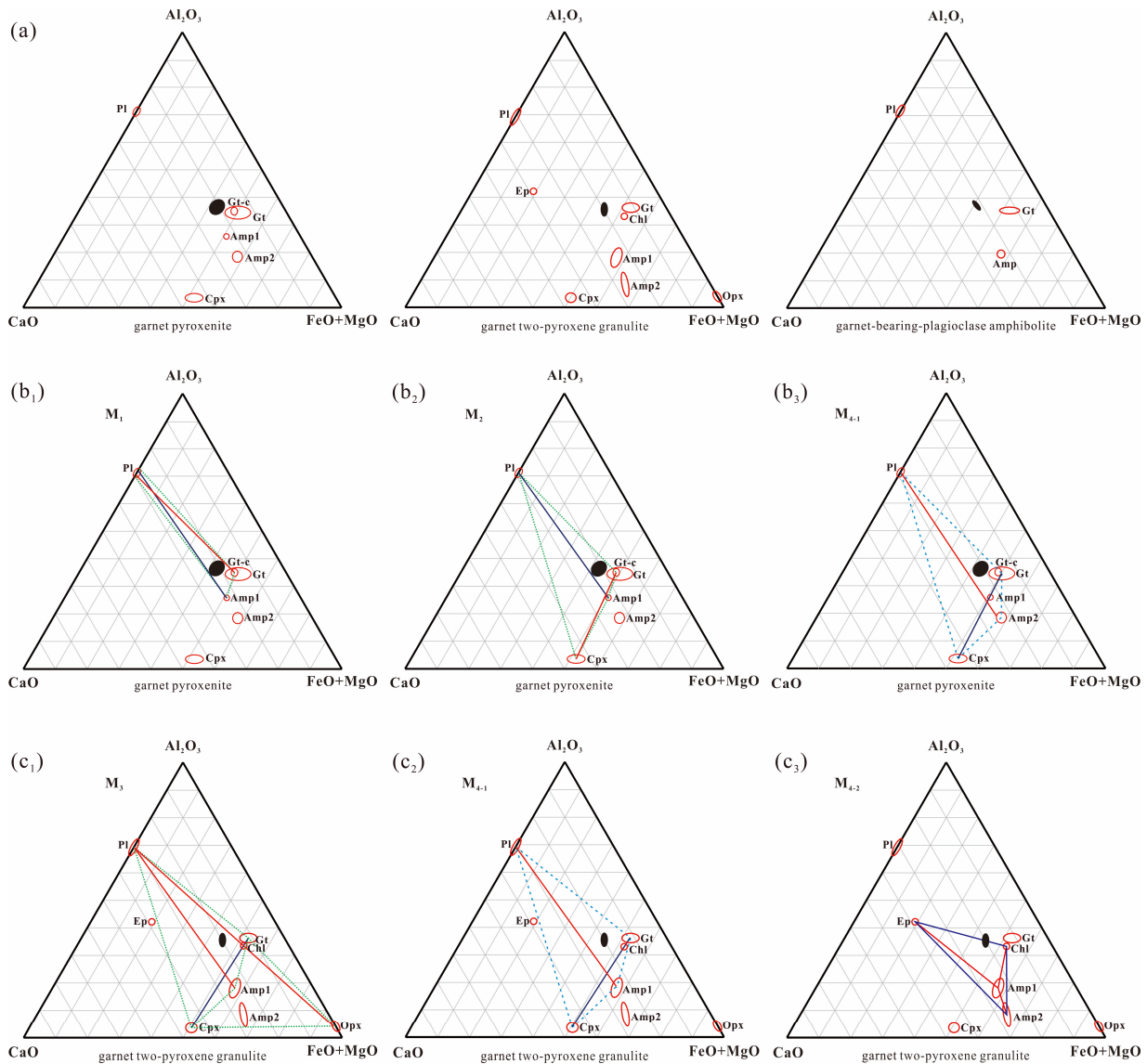


Figure 10. (a) ACF diagram between high-pressure granulite and mineral composition; (b) ACF metamorphic facies diagram of garnet–plagioclase–clinopyroxene; (c) ACF metamorphic facies diagram of garnet–amphibole. Blue line: reactants, Red line: products.

The garnet two-pyroxene granulite documents two stages of metamorphism. The mineral assemblage of the granulite facies stage (M_3) is $\text{Gt} + \text{Cpx} + \text{Opx} + \text{Amp}_1 + \text{Pl} + \text{Q}$ (Figure 10(c₁)), and possible metamorphic reactions in this stage are inferred to be: $\text{Gt} + \text{Cpx} + \text{Pl} \rightarrow \text{Gt} + \text{Cpx} + \text{Opx} + \text{Pl}$ and $\text{Gt} + \text{Cpx} + \text{Q} \rightarrow \text{Gt} + \text{Amp}_1 + \text{Pl}$. Based on the garnet rim and the composition in orthopyroxene without amphibole inclusions, the P-T conditions of the granulite facies stage are estimated to be $T = 912\sim 939\text{ }^\circ\text{C}$, $P = 8.1\sim 9.9\text{ kbar}$, which correspond to the granulite facies. The mineral assemblage of the early retrograde stage (M_{4-1}) is $\text{Amp}_1 + \text{Pl}_2 + \text{Q} + \text{Mag} \pm \text{Cpx}$, with a possible retrograde reaction being $\text{Gt} + \text{Cpx} + \text{Q} + \text{H}_2\text{O} \rightarrow \text{Amp}_1 + \text{Pl}_2 + \text{Mag}$ (Figure 10(c₂)). Based on the allotropic amphibole component in the matrix and the amphibole+plagioclase corona texture around garnet, the

P-T conditions of the early retrograde stage are $T = 661\sim 784\text{ }^{\circ}\text{C}$, $P = 3.1\sim 4.4\text{ kbar}$, which correspond to the amphibolite facies to granulite facies. The mineral assemblage of the late retrograde stage (M_{4-2}) is $\text{Amp} + \text{Ep} + \text{Chl}$, and the possible metamorphic reaction is $\text{Amp}_1 \rightarrow \text{Amp}_2 + \text{Ep} + \text{Chl}$ (Figure 10(c₃)). Based on the actinolite composition, we obtain the late retrograde stage conditions of $T = 637\sim 638\text{ }^{\circ}\text{C}$, $P = 1.1\sim 1.3\text{ kbar}$, which correspond to the high-greenschist to low-amphibolite facies.

The mineral assemblage of the garnet-bearing-plagioclase amphibolite in the early retrograde stage (M_{4-1}) is $\text{Amp} + \text{Pl} + \text{Q} + \text{Mag} \pm \text{Cpx}$, and based on the allotriomorphic amphibole component in the matrix and the amphibole + plagioclase corona texture around garnet, the P-T conditions of the early retrograde stage are $T = 722\sim 772\text{ }^{\circ}\text{C}$, $P = 4.1\sim 4.3\text{ kbar}$, which correspond to the granulite facies.

In summary, the P-T conditions of the M_1 stage in high-pressure granulites are $700\sim 706\text{ }^{\circ}\text{C}$, $6.0\sim 6.2\text{ kbar}$, which are equivalent to granulite facies; the P-T conditions of the M_2 stage are $854\sim 920\text{ }^{\circ}\text{C}$, $13.0\sim 13.8\text{ kbar}$ and are equivalent to high-pressure granulite facies; the P-T conditions of the M_3 stage are $912\sim 939\text{ }^{\circ}\text{C}$, $8.1\sim 9.9\text{ kbar}$, which are equivalent to granulite facies; the P-T conditions of the M_{4-1} stage are $661\sim 784\text{ }^{\circ}\text{C}$, $3.1\sim 4.4\text{ kbar}$, which are equivalent to granulite facies; the P-T conditions of the M_{4-2} stage are $637\sim 638\text{ }^{\circ}\text{C}$, $1.1\sim 1.3\text{ kbar}$, which are equivalent to the high-greenschist to low-amphibolite facies. The metamorphic P-T path (Figure 11) defines a clockwise P-T path with a nearly isothermal decompressional path (ITD) and slight heating after the peak stage (Figure 11).

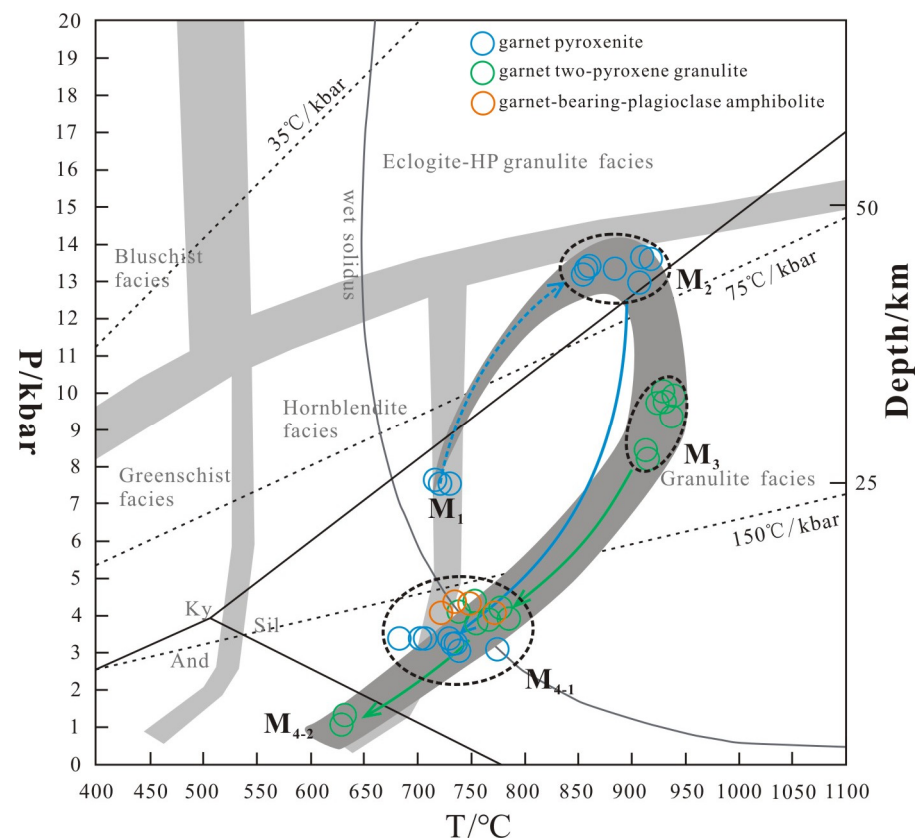


Figure 11. Temperature–pressure conditions and metamorphic P-T paths of high-pressure granulites from Yixian, Baoding.

7. Zircon LA-ICP-MS U-Pb Dating

A total of three samples were selected for U-Pb dating by LA-ICP-MS. Zircons were extracted at the Langfang Regional Geological Survey, Hebei Province, China. The acquisition of transmitted light reflected light and cathodoluminescence (CL) images was performed at Beijing GeoAnalysis Linghang Co. (Chinese Academy of Geological Sciences,

Beijing, China) Zircon LA-ICP-MS U-Pb was carried out at the Key Laboratory of Mineral Resources Evaluation in Northeast Asia, Ministry of Natural Resources, Jilin University, Changchun, China, using an ArF excimer laser system (GeoLas Pro, 193 nm wavelength) and a quadrupole ICP-MS (Agilent 7900) (Agilent Technologies, Inc., Santa Clara, CA, USA). Raw data were processed using the Glitter program. The data calculation and image rendering were processed using the ISOPLLOT (Version 3.0) program [61]. Uncertainties on individual analyses were reported with 1σ error and weighted mean ages were calculated at a 1σ confidence level, representing the 95% confidence interval. The results of U-Pb zircon dating are presented in Supplementary Table S7.

7.1. Garnet Pyroxenite

The zircons grains from garnet pyroxenite (samples Lg-0-01) are predominantly hypidiomorphic to allotriomorphic, with medium grain size and a 2:1 aspect ratio, while a few exhibited a 1:1 aspect ratio. The Th/U ratios of zircons from samples Lg-0-01 range from 0.003 to 0.070, consistent with the characteristics of metamorphic zircons. In zircon cathodoluminescence (CL) images, the majority display a homogeneous structure, and show broad banding, weak zoning, or no zoning with light luminescence, while some have bright cores with dark rims (Figure 12). Zircons with differential luminescence effects have brighter cores and darker rims, and the Th/U ratio is higher in the rims (0.013) than in the cores (0.011), consistent with metamorphic zircon.

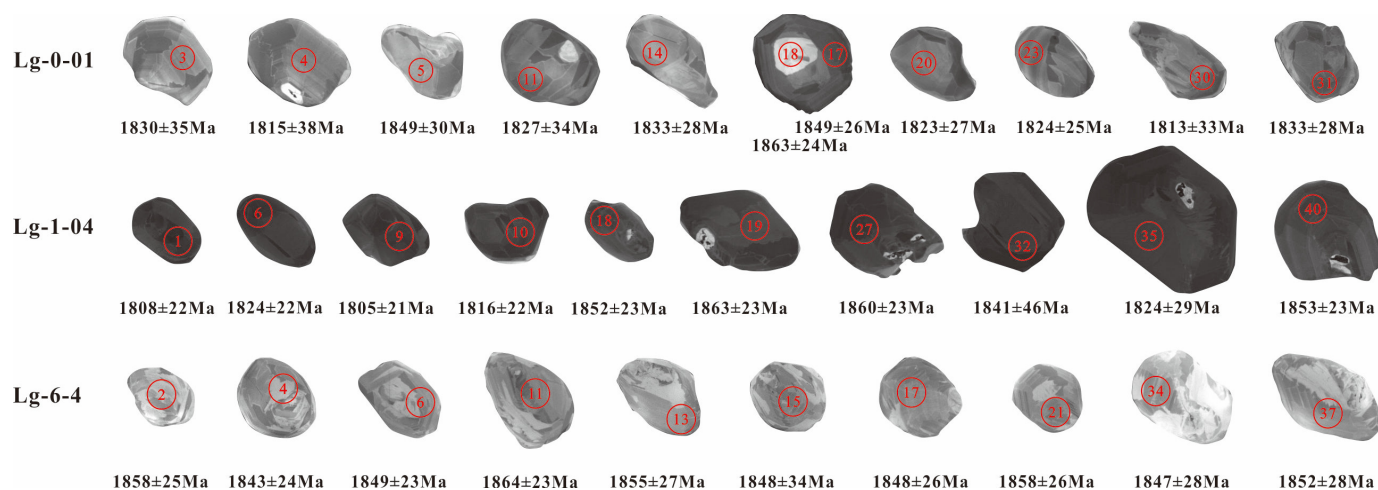


Figure 12. Representative cathodoluminescence (CL) images of zircons from samples Lg-0-01, Lg-1-04, and Lg-6-4, the red circles represent the locations of U-Pb analysis.

Results from 32 spot analyses in samples Lg-0-01 are presented in Supplementary Table S7 and show that all points are distributed on or near the concordia line. The data yield a weighted mean $^{207}\text{Pb}/^{206}\text{Pb}$ age of 1837 ± 10 Ma (MSWD = 0.28, $n = 32$) (Figure 13a) which we interpret as the timing of Paleoproterozoic metamorphism of these rocks.

7.2. Garnet Two-Pyroxene Granulite

The zircon grains from garnet two-pyroxene granulite (sample Lg-1-04) are hypidiomorphic to allotriomorphic, medium-grained, and with an aspect ratio of 2:1, while a few grains show a 1:1 aspect ratio. The Th/U ratios range from 0.001~0.069, indicating that they are metamorphic zircons. In the CL images, most zircons have a homogeneous structure with broad banding, weak zoning, or no zoning and light luminescence. The intensity of CL images differs between the core and the rim, with the core being brighter and having a slightly higher Th/U ratio than the rim. All zircons lack obvious oscillatory growth zoning.

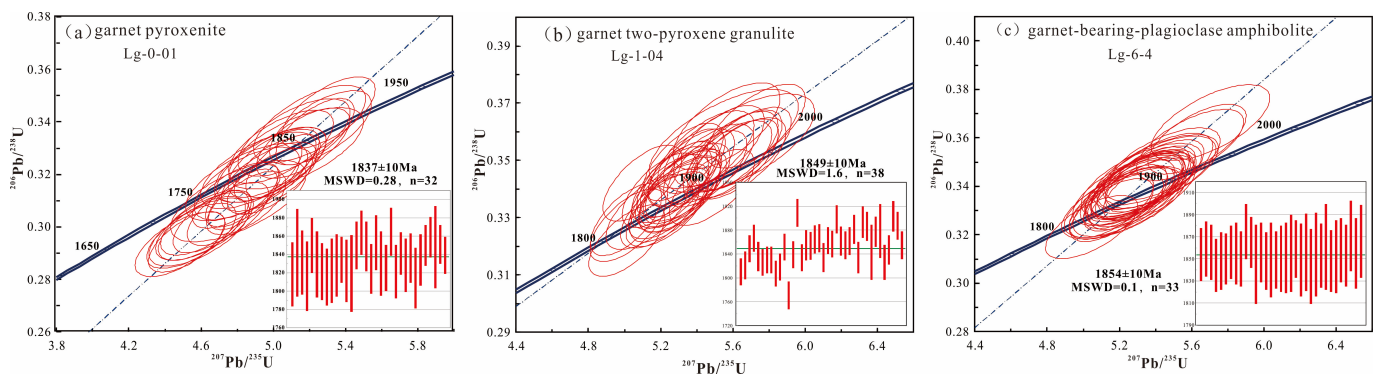


Figure 13. Zircon U-Pb concordia plot with weighted mean $^{207}\text{Pb}/^{206}\text{Pb}$ ages for samples Lg-0-01, Lg-1-04, Lg-6-4.

The results from 39 spot analyses in sample Lg-1-04 are shown in Supplementary Table S7. The data are distributed on or near the concordia line. The obtained weighted mean $^{207}\text{Pb}/^{206}\text{Pb}$ age for the samples was 1849 ± 10 Ma (MSWD = 1.6, $n = 38$) (Figure 13b). These results indicate that the garnet two-pyroxene granulite has undergone Paleoproterozoic metamorphism.

7.3. Garnet-Bearing-Plagioclase Amphibolite

The zircon grains from garnet-bearing-plagioclase amphibolite (sample Lg-6-4) are mostly allotriomorphic, with a ~1:1 aspect ratio. In the zircon CL images, most zircons have a homogeneous structure and display sectors and weak zoning with light luminescence (Figure 12). The Th/U ratios of zircons range from 0.004 to 0.009, consistent with the characteristics of metamorphic–genetic zircons.

A total of 33 points were analyzed for sample Lg-6-4, and the results are shown in Supplementary Table S7. The data are distributed on or near the concordia line in the concordia plot. The calculated weighted mean $^{207}\text{Pb}/^{206}\text{Pb}$ ages were 1854 ± 10 Ma (MSWD = 0.07, $n = 33$) (Figure 13c). We interpret this Paleoproterozoic age to mark the timing of metamorphism.

In summary, the zircons analyzed in this study display morphological characteristics and internal structures indicative of metamorphic growth. The features include broad banding, weak zoning, or no zoning, with some zircons having bright cores with dark rims. Our data yielded ages of 1837 ± 10 Ma, 1849 ± 10 Ma, and 1854 ± 10 Ma for high-pressure granulites and the retrograde products. These ages are consistent with the previously reported metamorphic ages of ~1850 Ma in the Fuping Complex [62–69].

8. Discussion

The Neoproterozoic strata exposed in the Yixian area are mainly the Yuanfang Formation of the Fuping Group, in which the high-pressure granulite samples were collected for this study with a peak high-pressure granulite facies mineral assemblage of $\text{Gt} + \text{Cpx} + \text{Pl} + \text{Q} \pm \text{Amp}$, which is consistent with the typical mineral assemblage of high-pressure mafic granulite. After the high-pressure granulite facies stage, orthopyroxene appeared in the normal granulite facies stage and the pressure decreased while the temperature increased slightly. The metamorphic condition of the retrograde stage ranges from high-amphibolite facies to granulite facies. With the appearance of epidote and chlorite in some samples and the composition of amphibole shifting to actinolite, the metamorphic condition reached from upper-greenschist to lower-amphibolite facies. According to the P-T conditions of the four metamorphic stages, a clockwise path with nearly isothermal (ITD) decompression and slight heating is inferred, which we correlated with the subduction–collision–uplift process associated with the assembly of the Eastern and Western Blocks of the NCC. In the early stage, the subduction and collision resulted in crust thickening, causing an increase in temperature and pressure, reaching the peak metamorphic high-pressure granulite facies.

Following the cessation of collision, the deeply buried rocks were rapidly exhumed as a concurrent result of isostasy, erosion, and other factors [49,70,71], with possible magmatic additions and extra heat input [72]. The garnet and the matrix clinopyroxene reacted to form the “white-eye socket” structure around the garnet, accompanied by symplectic intergrowth of Opx + Pl and Amp + Pl [52].

Previous studies in the Fuping Complex have also reported Late Paleoproterozoic metamorphic events with ages ranging from 1943 to 1802 Ma [73]. Meng et al. [52] reported that the mafic granulite in the Pingyang trondhjemitic gneiss underwent three stages of metamorphic evolution, in which the mineral assemblage of the peak stage was Gt + Cpx + Opx + Amp + Pl + Q, and the P-T conditions were 740~880 °C/11~14 kbar, indicating a clockwise P-T path with clear ITD segment. SIMS U-Pb dating of zircons of the trondhjemitic gneiss yielded a magmatic crystallization age of 2.52 Ga, and both the trondhjemitic gneiss and the mafic granulite enclaves yielded a metamorphic age of 1.89~1.86 Ga. Qian et al. [74] analyzed samples of garnet–mafic granulite from the Fuping County and inferred four-stage metamorphic mineral assemblages, the peak assemblage being Gt + Amp + Pl + Cpx + Ilm + Q, and the P-T conditions were 12~13 kbar/760~800 °C, yielding a near-isothermal clockwise P-T path. Metamorphic zircons in the Fuping HP mafic granulites show crystallization temperatures of 602~712 °C and SIMS zircon U-Pb ages of 1891 ± 14 Ma and 1849 ± 6 Ma, interpreted to represent the cooling stage. Liu et al. [75] investigated the mafic granulites exposed in the TTG gneisses in the Daliushu area, delineating four metamorphic stages with the peak mineral assemblage of Gt + Cpx + Opx + Amp + Pl + Q + Zr + Ilm and obtaining the P-T conditions of 680~820 °C/7.2~11.7 kbar. The P-T paths are clockwise with near-isothermal decompression (ITD) and subsequent near-isobaric cooling (IBC) segments. The metamorphic zircons yield a weighted mean age of 1849 ± 9 Ma, which is consistent with the metamorphic time of surrounding TTG gneisses.

The results of the present study are similar to the above and show that the Fuping Complex underwent regional metamorphism ~1.85 Ga, which may be related to the collision between continental blocks in the NCC [34,47,75].

Previous studies in the TNCO have reported similar ~1.85Ga collisional metamorphic evolution (Figure 14), including from the Huai’an Complex [76,77], the Xuanhua Complex [24,73], the Hengshan Complex [78,79], the Zhanhuang Complex, etc. The HP granulite samples from Xuanhua Xiwangshan have a clockwise P-T path and near-isothermal decompression. The whole-rock–single-mineral Sm-Nd and $^{40}\text{Ar}/^{39}\text{Ar}$ dating of garnet shows an age of ~1.85 Ga. This result is also attested in subsequent studies [19,74,80]. Metamorphic ages of ~1850 Ma have been reported from different rock types of the Huai’an Complex by using different chronological methods [23,33,81–83], in which the metamorphic trajectories show clockwise features, and the Late Paleoproterozoic regional metamorphism is correlated to the subduction–collision process between the Eastern and Western Blocks of the NCC. The metamorphic ages reported in the Hengshan Complex are mainly in the range of 1830–1886 Ma [10,84,85] with similar metamorphic stages [25,34,77,78,86,87]. The metamorphic rocks of the Jiehekou Group in the Lvliang Complex are generally upper amphibolite facies and local granulite facies [25,88,89]. At least two sets of metamorphic ages (~2.5 Ga and ~1.85 Ga) are recognized, of which the ~1.85 Ga age is interpreted as a record of regional metamorphism associated with the collision between the Eastern and Western Blocks [35,88,90].

In general, the metamorphic complexes in the TNCO have a similar clockwise metamorphic PT path, followed by near-isothermal decompression, reflecting a collisional orogenic environment that is closely related to the subduction–collision–exhumation during the assembly of the Eastern and Western Blocks of the NCC. Combined with the results of the Fuping high-pressure granulite in this study, we propose the following scenario for the high-pressure metamorphism in the TNCO. During the Late Paleoproterozoic at ~1.85 Ga, subduction and collision between the Eastern and Western Blocks occurred (Figure 15a,b). The collision caused the thickening of the crust, resulting in a slow increase in temperature and a rapid increase in pressure, and the complex underwent medium-

to high-pressure granulite facies metamorphism in the lower crust (e.g., the Hengshan, Huaian, Fuping, and Taihua domains). Following peak metamorphism, the thickened crust underwent exhumation driven by crustal isostatic compensation and accompanying decompression, with a rapid pressure drop at near-constant temperature (Figure 15d). Finally, the rocks underwent retrograde metamorphism when the crust was exhumed to shallow levels (Figure 15e) [25].

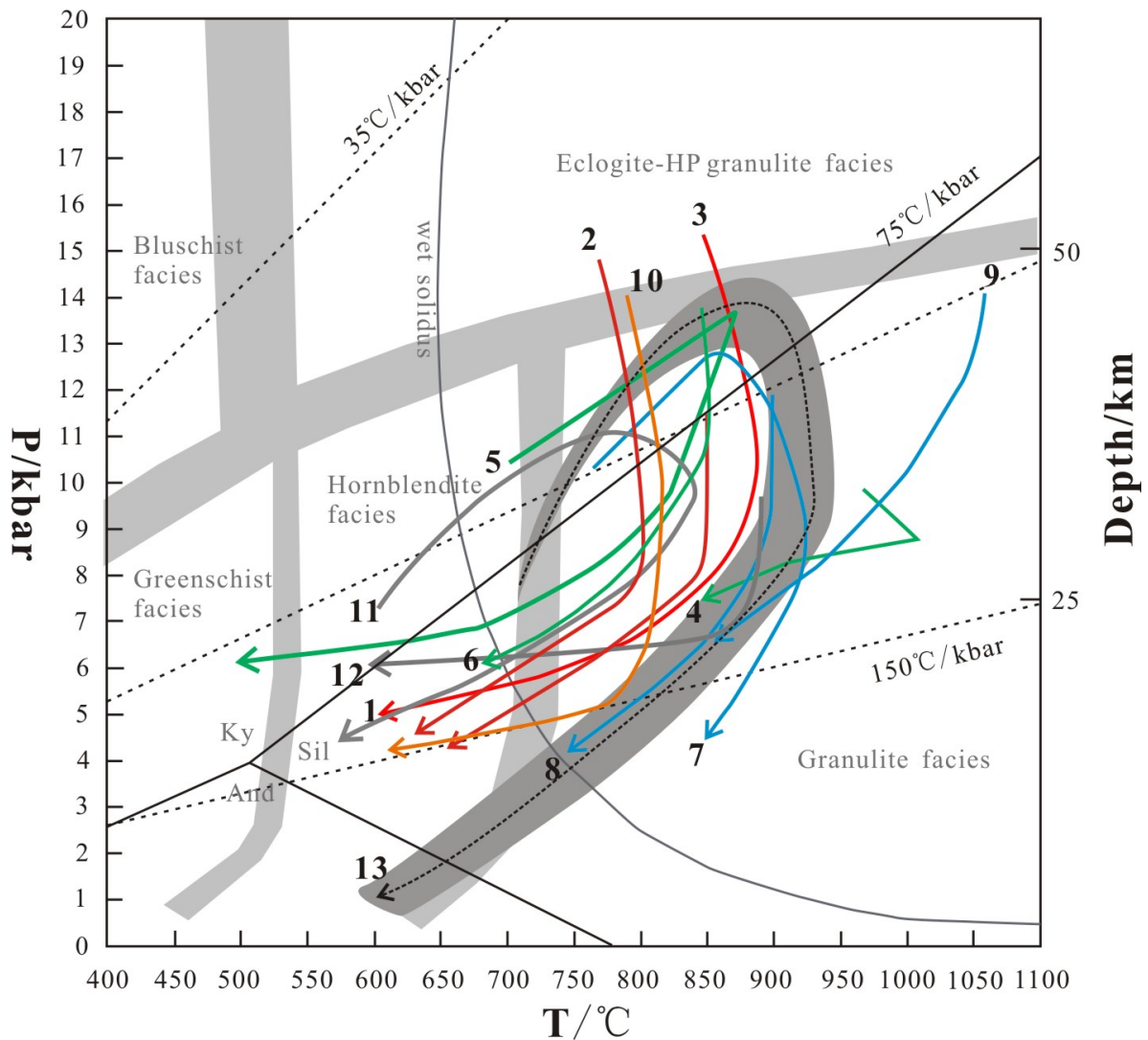


Figure 14. Metamorphic P-T paths of the high-pressure granulites from the TNCO. 1: Hengshan [87]; 2: Hengshan [25]; 3: Hengshan [91]; 4: Huai'an Huangtuyao [92]; 5: Huai'an Manjinggou [18]; 6: Huai'an [93]; 7: Xuanhua Dadonggou [94]; 8: Xuanhua Xiwangshan [95]; 9: Xuanhua Xiwangshan [96]; 10: Chengde [80]; 11: Fuping [24]; 12: Fuping [25]; 13: data for this research.

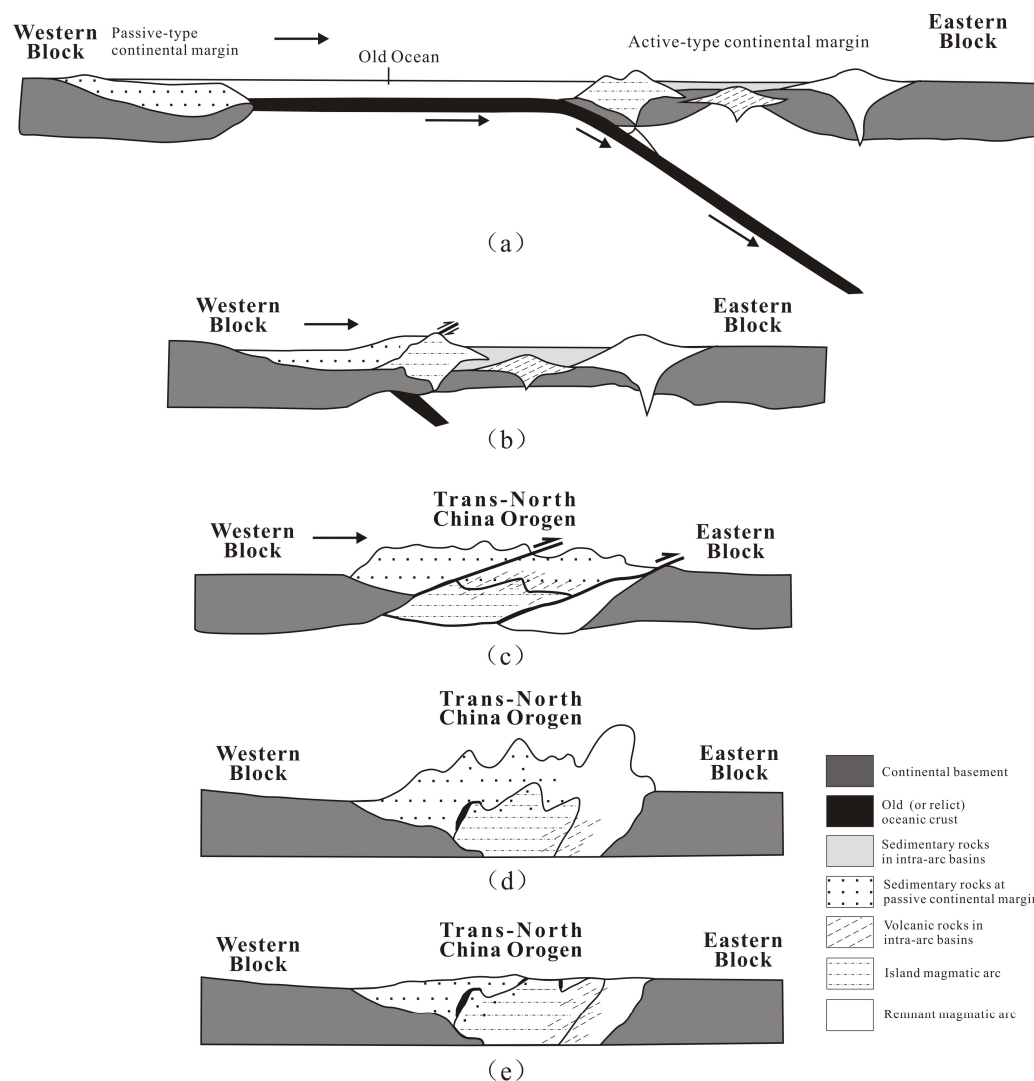


Figure 15. A series of schematic sections showing the proposed tectono-thermal evolution of the Fuping high-pressure granulite (modified after [25]). (a) During the Late Paleozoic at about 1.85 Ga, the Western Block subducted into the Eastern Block. (b) Collision between Eastern and Western Block. (c) Thickening of the crust, the complex underwent medium- to high-pressure granulite facies metamorphism in the lower crust. (d) Thickening of the crust, underwent exhumation driven by crustal isostatic compensation and accompanying decompression, with a rapid pressure drop at near-constant temperature. (d) The rocks underwent retrograde metamorphism when the crust was exhumed to shallow level.

9. Conclusions

1. The Yixian high-pressure granulites experienced a prograde stage (M_1) of metamorphism at 700~706 °C and 6.0~6.2 kbar; high-pressure granulite facies stage (M_2) of 854~920 °C, 13.0~13.8 kbar; granulite facies stage (M_3) at 912~939 °C, 8.1~9.9 kbar; an early retrograde stage (M_{4-1}) at 661~784 °C, 3.1~4.4 kbar; and a late retrograde stage M_{4-2} of 637~638 °C, 1.1~1.3 kbar, along a near-isothermal decompression (ITD) path with slight heating after the peak stage.
2. The metamorphic zircons in Yixian high-pressure granulites yielded $^{207}\text{Pb}/^{206}\text{Pb}$ ages of 1837 ± 10 Ma, 1849 ± 10 Ma, and 1854 ± 10 Ma, which can be interpreted to mark the peak to retrograde stages of metamorphism. The protoliths of the Yixian high-pressure granulites may have originated in an island arc environment and were involved in the collision between the Eastern and Western Blocks of the NCC at ~1.85 Ga.

Supplementary Materials: The following supporting information can be downloaded at: <https://www.mdpi.com/article/10.3390/min14020138/s1>, Supplementary Table S1: Major (wt.%) element compositions of the representative high-pressure granulites analyzed in the present study. Supplementary Table S2: Trace and rare earth element (ppm) compositions of the representative high-pressure granulites analyzed in the present study. Supplementary Table S3: Selected microprobe analyses for garnet of high-pressure granulites in this study. Supplementary Table S4: Selected microprobe analyses for clinopyroxene of high-pressure granulites in this study. Supplementary Table S5: Selected microprobe analyses for amphibole of high-pressure granulites in this study. Supplementary Table S6: Selected microprobe analyses for plagioclase of high-pressure granulites in this study. Supplementary Table S7: U-Pb isotopic analyses for representative zircons of high-pressure granulites.

Author Contributions: Conceptualization, Z.Z., C.Z. and C.L.; Methodology, C.Z. and C.L.; software, Z.Z.; validation, Z.Z., C.Z. and M.S.; formal analysis, Z.Z.; investigation, Z.Z., C.Z., J.H. (Junjie Hao), L.D., J.H. (Jianjun Hou), F.H. and M.L.; resource, C.Z. and L.D.; data curation, Z.Z.; writing—original draft preparation Z.Z.; writing—review and editing, C.Z., C.L. and M.S.; visualization, Z.Z.; supervision, C.Z. and C.L.; project administration, C.Z.; funding acquisition, C.Z. and C.L. All authors have read and agreed to the published version of the manuscript.

Funding: This study was financially supported by the National Natural Science Foundation of China (No. 42172213 and 41972215).

Data Availability Statement: All data used in this study are available in the main text and the Supplementary Materials.

Acknowledgments: We would like to express our gratitude to Key Laboratory of Mineral Resources Evaluation of Northeast Asia, Ministry of Land and Resources of China, for their support with the microprobe analysis and LA-ICP-MS U-Pb zircon dating. We are grateful to the anonymous reviewers who helped improve the paper and the editors for handling, editing, and advising.

Conflicts of Interest: Authors, Junjie Hao, Lishuai Dong, Feifei Hou, and Meihui Li are employed by the Geological Team of Hebei Bureau of Geology and Mineral Resources Exploration. The remaining authors declare that the research was conducted in the absence of any commercial or financial relationships that could be construed as a potential conflict of interest.

References

- Gerya, T.V.; Perchuk, L.L.; Triboulet, C.; Audren, C.; Sezko, A.L. Petrology of the Tumanshet Zonal Metamorphic Complex, Eastern Sayan. *Petrology* **1997**, *5*, 503–533. [[CrossRef](#)]
- Lal, R.K. Internally consistent recalibrations of mineral equilibria for geothermobarometry involving garnet–orthopyroxene–plagioclase–quartz assemblages and their application to the South Indian granulites. *J. Metamorph. Geol.* **1993**, *11*, 855–866. [[CrossRef](#)]
- Santosh, M.; Liu, D.Y.; Shi, Y.R.; Liu, S.J. Paleoproterozoic accretionary orogenesis in the North China Craton: A SHRIMP zircon study. *Precambrian Res.* **2013**, *227*, 29–54. [[CrossRef](#)]
- Tang, X.; Zhai, F.; Sheng, X. The Roles of β -Integrin of Chinese Shrimp (*Fenneropenaeus chinensis*) in WSSV Infection. *Int. J. Mol. Sci.* **2017**, *18*, 1465. [[CrossRef](#)] [[PubMed](#)]
- Yang, C.H.; Du, L.L.; Wan, Y.S.; Liu, Z.X. SHRIMP Zircon U-Pb Chronology of Tonalitic Gneiss in Banqiaogou Area, Pingshan County, Hebei Province. *Geol. J. China Univ.* **2004**, *10*, 514–522, (In Chinese with English Abstract).
- Zhao, G.C.; Wilde, S.A.; Cawood, P.A.; Lu, L.Z. Thermal evolution of the Archaean basement rocks from the eastern part of the North China Craton and its bearing on tectonic setting. *Int. Geol. Rev.* **1998**, *40*, 706–721. [[CrossRef](#)]
- Zhao, L.; Zhang, J.J.; Liu, S.W. Syn-deformational granites of the Longquanguan ductile shear zone and their monazite electron microprobe dating. *Acta Petrol. Mineral.* **2006**, *25*, 210–218, (In Chinese with English Abstract).
- Tang, L.; Santosh, M. Neoproterozoic terrane assembly and Wilson cycle in the North China Craton: An overview from the central segment of the Trans North China Orogen. *Earth-Sci. Rev.* **2018**, *182*, 1–27. [[CrossRef](#)]
- Tian, Y.Q.; Liang, Y.F.; Fan, S.K.; Zhu, B.Q.; Chen, L.W. Chronology and Nd isotope evolution of the Hengshan Complex. *Geochimica* **1992**, *3*, 255–264. (In Chinese) [[CrossRef](#)]
- Trap, P.; Faure, M.; Lin, W.; Bruguier, O.; Monié, P. Contrasted tectonic styles for the Paleoproterozoic evolution of the North China Craton: Evidence for a ~2.1Ga thermal and tectonic event in the Fuping Massif. *J. Struct. Geol.* **2008**, *30*, 1109–1125. [[CrossRef](#)]
- Zhang, J.; Zhao, G.C.; Sun, M.; Wilde, S.A.; Li, S.Z.; Liu, S.W. High-pressure mafic granulites in the Trans-North China Orogen: Tectonic significance and age. *Gondwana Res.* **2006**, *9*, 349–362. [[CrossRef](#)]
- Guo, J.H.; Chen, F.K.; Zhang, X.M.; Siebel, W. Evolution of syn- to post-collisional magmatism from north Sulu UHP belt, eastern China: Zircon U-Pb geochronology. *Acta Petrol. Sin.* **2005**, *21*, 1281–1301, (In Chinese with English Abstract).

13. Zhao, G.C.; Sun, M.; Wilde, S.A.; Li, S.Z. Neoproterozoic to Palaeoproterozoic evolution of the North China Craton: Key issues revisited. *Precambrian Res.* **2005**, *136*, 177–202. [[CrossRef](#)]
14. Irvine, T.N.; Baragar, W.R.A. A guide to the chemical classification of the common volcanic rocks. *Can. J. Earth Sci.* **1971**, *8*, 523–548. [[CrossRef](#)]
15. O'Brien, P.J.; Walte, N.; Li, J.H. The petrology of two distinct granulite types in the Hengshan Mts, China, and tectonic implications. *J. Asian Sci.* **2005**, *24*, 615–627. [[CrossRef](#)]
16. Pearce, J.A. Geochemical fingerprinting of oceanic basalts with applications to ophiolite classification and the search for Archean oceanic crust. *Lithos* **2008**, *100*, 14–48. [[CrossRef](#)]
17. Guo, J.H.; Wang, S.S.; Sang, H.Q. ⁴⁰Ar–³⁹Ar age spectra of garnet porphyroblast: Implications for metamorphic age of high-pressure granulite in the North China craton. *Acta Petrol. Sin.* **2001**, *17*, 436–442, (In Chinese with English Abstract).
18. Harley, S.L. An experimental study of the partitioning of Fe and Mg between garnet and orthopyroxene. *Contrib. Mineral. Petrol.* **1984**, *86*, 359–373. [[CrossRef](#)]
19. Zhai, M.G.; Guo, J.H.; Li, J.H. The discovery and implications of receding metamorphic gabbro in North China. *Chin. Sci. Bull.* **1995**, *40*, 1590–1594. (In Chinese)
20. Cheng, Y.Q.; Yang, C.H.; Wan, Y.S.; Liu, Z.X.; Zhang, X.P.; Du, L.L.; Zhang, S.G.; Wu, J.S.; Gao, J.F. *Precambrian Geology and Anatexis and Its Reworking in the Crustal Rocks at the Central-Northern Segments of the Taihangshan Mountain*; Geological Publishing House: Beijing, China, 2004; 191p, (In Chinese with English Abstract).
21. Liu, J.H.; Wang, J.; Li, Z.M.; Wu, C.M. Paleoproterozoic medium to high pressure metamorphism in the Wanzi supracrustal association, Trans-North China orogen: New insights from the gedrite-bearing gneiss, gedrite-free gneiss, and amphibolite. *Precambrian Res.* **2021**, *360*, 106248. [[CrossRef](#)]
22. Ludwig, K.R. *User's Manual for Isoplot/Ex Version 3.00, a Geochronological Toolkit for Microsoft Excel*; Berkeley Geochronology Center Special Publications: Berkeley, CA, USA, 2003; Volume 4, 72p.
23. Yan, Y.H.; Guo, J.H.; Liu, W.J. Study on Metamorphic Mineral Garnet and its Balanced Symbiotic Relationship with Monoclinopene in Granulite Facies Belt of North China. *Acta Petrol. Sin.* **1998**, *14*, 471–480, (In Chinese with English Abstract).
24. Liu, S.W.; Pan, Y.M.; Li, J.H.; Li, Q.G.; Zhang, J. Geological and isotopic geochemical constraints on the evolution of the Fuping Complex, North China Craton. *Precambrian Res.* **2002**, *117*, 41–56. [[CrossRef](#)]
25. Zhao, G.C.; Wilde, S.A.; Cawood, P.A.; Sun, M. Archean blocks and their boundaries in the North China Craton: Lithological, geochemical, structural and P-T path constraints and tectonic evolution. *Precambrian Res.* **2001**, *107*, 45–73. [[CrossRef](#)]
26. Wei, C.J. Granulite facies metamorphism and petrogenesis of granite (II): Quantitative modeling of the HT–UHT phase equilibria for metapelites and the petrogenesis of S-type granite. *Acta Petrol. Sin.* **2016**, *32*, 1625–1643, (In Chinese with English Abstract).
27. The State Administration of Quality Supervision Inspection and Quarantine of the People's Republic of China, China National Standardization Management Committee. *GB/T 14506.30-2010; Methods of chemical analysis of silicate rocks—Part 30: Determination of 44 elemental*. China Standards Press: Beijing, China, 2010. (In Chinese)
28. Dong, X.F.; Tang, Z.C.; Chen, Z.D.; Yu, S.Q.; Zhao, X.D.; Zhou, Z.Y.; Wu, X.Y.; Xiao, Q.H. Geochemical characteristics of the basic and magnesian metamorphic rocks in Longyou Area, Zhejiang province and their tectonic setting. *Earth Sci.* **2016**, *14*, 1322–1333, (In Chinese with English Abstract).
29. Morimoto, N.; Fabries, J.; Ferguson, A.K.; Ginzburg, I.V.; Ross, M.; Seifert, F.A.; Zussman, J.; Aoki, K.; Gottardi, G. Nomenclature of pyroxenes. *Am. Mineral.* **1988**, *73*, 1123–1133.
30. Boynton, W.V. Geochemistry of the rare earth elements: Meteorite studies. *Rare Earth Elem. Geochem.* **1984**, *2*, 63–114. [[CrossRef](#)]
31. Tang, L.; Santosh, M.; Teng, X.M. Paleoproterozoic (ca. 2.1–2.0 Ga) arc magmatism in the Fuping Complex: Implications for the tectonic evolution of the Trans–North China orogen. *Precambrian Res.* **2015**, *268*, 16–32. [[CrossRef](#)]
32. Chu, H.; Wang, H.C.; Wei, C.J.; Liu, H.; Zhang, K. The Metamorphic Evolution History of High Pressure Granulites in Chengde Area, Northern Margin of North China: Zircon Chronology and Geochemical Evidence. *Acta Geosci. Sin.* **2012**, *33*, 977–987, (In Chinese with English Abstract).
33. Shaw, D.M. The origin of Apsley gneiss, Ontario. *Can. J. Earth Sci.* **1972**, *9*, 18–35. [[CrossRef](#)]
34. Yin, X.Q. *The Petrological Characteristics and the Protolith of High-Pressure Granulite of Chicheng and Xuanhua, North Hebei Province*; Chengdu University of Technology: Chengdu, China, 2016.
35. Verma, S.P.; Guevara, M.; Agrawal, S. Discrimination four tectonic settings: Five new geochemical diagrams for basic and ultrabasic volcanic rocks based on log-ratio transformation of major-element data. *J. Earth Syst. Sci.* **2006**, *115*, 485–528. [[CrossRef](#)]
36. Li, Y. *The P-T Trajectory of Xuanhua Basal High-Pressure Sepiolite in Hebei and Its Geological Significance*; China University of Geosciences (Beijing): Beijing, China, 2020. (In Chinese)
37. Ito, K.; Kennedy, G.C. An experimental study of the basalt-garnet granulite-eclogite transition. In *The Structure and Physical Properties of the Earth's Crust*; Monograph no.14; Heacock, J.G., Ed.; American Geophysical Union: Washington, DC, USA, 1971; pp. 303–314.
38. Zhai, M.G. Two kinds of granulites (HT-HP and HT-UHT) in North China Craton: Their genetic relation and geotectonic implications. *Acta Petrol. Sin.* **2009**, *25*, 1753–1771, (In Chinese with English Abstract).
39. Peng, P.; Zhai, M.G.; Zhang, H.F.; Guo, J.H. Geochronological constraints on Proterozoic evolution of the North China Block: SHRIMP zircon ages of different types of mafic dykes. *Int. Geol. Rev.* **2005**, *47*, 492–508. [[CrossRef](#)]

40. Holland, T.; Blundy, J. Non-Ideal Interactions in Calcic Amphiboles and Their Bearing on Amphibole-Plagioclase Thermometry. *Contrib. Mineral. Petrol.* **1994**, *116*, 433–447. [[CrossRef](#)]
41. Carswell, D.A.; Wilson, R.N.; Zhai, M. Metamorphic evolution, mineral chemistry and thermobarometry of schists and orthogneisses hosting ultra-high pressure eclogites in the Dabieshan of central China. *Lithos* **2000**, *52*, 121–155. [[CrossRef](#)]
42. Trap, P.; Faure, M.; Lin, W.; Monié, P. Late Paleoproterozoic (1900–1800 Ma) nappe stacking and polyphase deformation in the Hengshan-Wutaishan area: Implications for the understanding of the Trans-North-China Belt. North China Craton. *Precambrian Res.* **2007**, *156*, 85–106. [[CrossRef](#)]
43. Anderson, D.E.; Olimpio, J.C. Progressive homogenization of metamorphic garnets, South Morar, Scotland: Evidence for volume diffusion. *Can. Mineral.* **1977**, *15*, 205–216.
44. Xia, Q.X.; Zheng, Y.F. The composition and chemical zoning in garnet from high to ultrahigh metamorphic rocks. *Acta Petrol. Sin.* **2011**, *27*, 433–450, (In Chinese with English Abstract).
45. Nimis, P.; Taylor, W.R. Single clinopyroxene thermobarometry for garnet peridotites Part, I. Calibration and testing of a Cr-in-Cpx barometer and an enstatite-in-Cpx thermometer. *Contrib. Mineral. Petrol.* **2000**, *139*, 541–554. [[CrossRef](#)]
46. Kröner, A.; Wilde, S.A.; Li, J.H.; Wang, K.Y. Age and evolution of a Late Archean to Early Palaeoproterozoic upper to lower crustal section in the Wutaishan/Hengshan/Fuping terrain of northern China. *J. Asian Earth Sci.* **2005**, *24*, 577–595. [[CrossRef](#)]
47. Middlemost, E.A.K. Naming Materials in the Magma/Igneous Rock System. *Earth-Sci. Rev.* **1984**, *37*, 215–224. [[CrossRef](#)]
48. Enami, M. Pressure-temperature path of Sanbagawa prograde metamorphism deduced from grossular zoning of garnet. *J. Metamorph. Geol.* **1998**, *16*, 97–106. [[CrossRef](#)]
49. Spear, F.S. *Metamorphic Phase Equilibria and Pressure–Temperature–Time Paths*; Mineralogical Society of America: Washington, DC, USA, 1993; p. 799.
50. Anovitz, L.M. Al zoning in pyroxene and plagioclase: Windows on late prograde to early retrograde P-T paths in granulite terranes. *Am. Mineral.* **1991**, *76*, 1328–1343.
51. Yang, F.; Sontosh, M.; Kim, S.W.; Zhou, H.Y. Late Neoproterozoic to Paleoproterozoic arc magmatism in the Shandong Peninsula, North China Craton and its tectonic implications. *Precambrian Res.* **2021**, *358*, 106188. [[CrossRef](#)]
52. Meng, J.; Peng, T.; Liu, J.H.; Zhang, H.C.; Wang, G.D.; Lu, J.S.; Chen, H.X.; Wang, H.Y.; Zhang, Q.W.; Wu, C.M. Metamorphic Evolution and SIMS Zircon U-Pb Geochronology of Mafic Granulite and Amphibolite Enclaves of the Pingyang Trondhjemitic Pluton, Fuping Terrane, North China. *Precambrian Res.* **2017**, *303*, 75–90. [[CrossRef](#)]
53. Caddick, M.J.; Konopásek, J.; Thompson, A.B. Preservation of garnet growth zoning and the duration of prograde metamorphism. *J. Petrol.* **2010**, *51*, 2327–2347. [[CrossRef](#)]
54. Dahl, P.S. The thermal-compositional dependence of Fe²⁺-Mg distributions between coexisting garnet and pyroxene: Applications to geothermometry. *Am. Mineral.* **1980**, *65*, 852–866.
55. Eckert, J.O., Jr.; Newton, R.C.; Kleppa, O.J. The ΔH of reaction and recalibration of garnet-pyroxene-plagioclase-quartz geobarometers in the CMAS system by solution calorimetry. *Am. Mineral.* **1991**, *76*, 148–160.
56. Aranovich, L.Y.; Berman, R.G. A new garnet-orthopyroxene thermometer based on reversed Al₂O₃ solubility in FeO-Al₂O₃-SiO₂ orthopyroxene. *Am. Mineral.* **1997**, *82*, 345–353. [[CrossRef](#)]
57. Harley, S.L. The solubility of alumina in orthopyroxene coexisting with garnet in FeO-MgO-Al₂O₃-SiO₂ and CaO-FeO-MgO-Al₂O₃-SiO₂. *J. Petrol.* **1984**, *25*, 665–696. [[CrossRef](#)]
58. Leake, B.E.; Woolley, A.R.; Arps, C.E.S.; Birch, W.D.; Gilbert, M.C.; Grice, J.D.; Hawthorne, F.C.; Kato, A.; Kisch, H.J.; Krivovichev, V.G.; et al. Nomenclature of amphiboles: Report of the Subcommittee on Amphiboles of the International Mineralogical Association, Commission on New Minerals and Mineral Names. *Can. Mineral.* **1997**, *35*, 219–246.
59. Green, D.H.; Ringwood, A.E. An experimental investigation of the gabbro to eclogite transformation and its petrological applications. *Geochim. Cosmochim. Acta* **1967**, *31*, 767–833. [[CrossRef](#)]
60. Huang, G.Y.; Brown, M.; Guo, J.H.; Piccoli, P.; Zhang, D.D. Challenges in constraining the P-T conditions of mafic granulites: An example from the northern Trans-North China Orogen. *J. Metamorph. Geol.* **2018**, *36*, 739–768. [[CrossRef](#)]
61. Ma, J.; Wang, R.M. Discovery and geological significance of blueschist-anorthoclase feldspar assemblages in the Xuanhua-Chi Cheng high-pressure sepiolite belt. *Acta Petrol. Sin.* **1995**, *3*, 273–278. (In Chinese)
62. Guan, H.; Sun, M.; Wilde, S.A.; Zhou, X.H.; Zhai, M.G. SHRIMP U-Pb zircon geochronology of the Fuping Complex: Implications for formation and assembly of the North China Craton. *Precambrian Res.* **2002**, *113*, 1–18. [[CrossRef](#)]
63. Guo, J.H.; Zhai, M.G.; Zhang, Y.G.; Li, Y.G.; Yan, Y.H. Geological features, petrology and isotopic chronology of the earlier Cambrian high-pressure sepiolite mélange belt in Huai’an Manjinggou. *Acta Petrol. Sin.* **1993**, *9*, 329–341. (In Chinese) [[CrossRef](#)]
64. Li, Q.; Santosh, M.; Li, S.R.; Guo, P. The formation and rejuvenation of continental crust in the central North China Craton: Evidence from zircon U-Pb geochronology and Hf isotope. *J. Asian Earth Sci.* **2014**, *95*, 17–32. [[CrossRef](#)]
65. Liu, D.Y.; Nutman, A.P.; Compston, W.; Wu, J.S.; Shen, Q.H. Remnants of ≥ 3800 Ma crust in the Chinese part of the Sino-Korean craton. *Geology* **1992**, *20*, 339–342. [[CrossRef](#)]
66. Sun, S.S.; McDonough, W.F. Chemical and Isotopic Systematics of Oceanic Basalts: Implications for Mantle Composition and Processes. *Geol. Soc. Spec. Publ.* **1989**, *42*, 313–345. [[CrossRef](#)]
67. Trap, P.; Faure, M.; Lin, W.; Meffre, S. The Lüliang Massif: A key area for the understanding of the Palaeoproterozoic Trans-North China Belt, North China Craton. *Geol. Soc. Lond. Spec. Publ.* **2009**, *323*, 99–125. [[CrossRef](#)]

68. Yardley, B.W.D. The nature and significance of the mechanism of silimanite growth in the Connemara Schists, Ireland. *Contrib. Miner. Petrol.* **1977**, *65*, 53–58. [[CrossRef](#)]
69. Zhang, J.; Zhao, G.C.; Li, S.Z.; Sun, M.; Chan, L.S.; Shen, W.L.; Liu, S.W. Structural pattern of the Wutai Complex and its constraints on the tectonic framework of the Trans-North China Orogen. *Precambrian Res.* **2012**, *222–223*, 212–229. [[CrossRef](#)]
70. England, P.C.; Thompson, A.B. Pressure–temperature–time paths of regional metamorphism, I. Heat transfer during the evolution of thickened continental crust. *J. Petrol.* **1984**, *25*, 894–928. [[CrossRef](#)]
71. Wei, G.; Kong, F.; Liu, H.; Wang, X.M.; Zhang, Y.C.; Liu, X.H. Petrology, Metamorphic P-T Paths and Zircon U-Pb Ages for Paleoproterozoic Mafic Granulites from Xuanhua, North China Craton. *J. Earth Sci.* **2019**, *30*, 1197–1214. [[CrossRef](#)]
72. Hansen, B. The transition from pyroxene granulite facies to garnet clinopyroxene granulite facies: Experiments in the system CaO-MgO-Al₂O₃-SiO₂. *Contrib. Mineral. Petrol.* **1981**, *76*, 234–242. [[CrossRef](#)]
73. Du, L.L.; Yang, C.H.; Song, H.X.; Wang, J.L.; Duan, Q.S.; Huang, Z.Q.; Cheng, H.F.; Geng, Y.S.; Ren, L.D. Neoproterozoic–Paleoproterozoic multi-stage geological events and their tectonic implications in the Fuping Complex, North China Craton. *Earth Sci.* **2020**, *45*, 3179–3195, (In Chinese with English Abstract).
74. Qian, J.; Yin, C.; Zhang, J.; Ma, L.; Wang, L. High-Pressure Granulites in the Fuping Complex of the Central North China Craton: Metamorphic P-T-t Evolution and Tectonic Implications. *J. Asian Earth Sci.* **2018**, *154*, 255–270. [[CrossRef](#)]
75. Liu, J.H.; Zhang, Q.W.; Wang, J.; Zhang, H.C.; Wu, C.M. Metamorphic evolution and SIMS U-Pb geochronology of orthopyroxene-bearing high-P semipelitic granulite in the Fuping area, middle Trans-North China orogen. *J. Metamorph. Geol.* **2021**, *39*, 297–320. [[CrossRef](#)]
76. Wang, R.M.; Chen, Z.Z.; Chen, F. Grey gneiss and high-pressure sepiolite inclusions in Heng Shan and their geological significance. *Acta Petrol. Sin.* **1991**, *7*, 36–45. (In Chinese)
77. Zhang, H.F.; Zhai, M.G.; Peng, P. Zircon SHRIMP U-Pb age of the Paleoproterozoic high-pressure granulites from the Sanggan area, the North China Craton and its geologic implications. *Earth Sci. Front.* **2006**, *13*, 190–199, (In Chinese with English Abstract).
78. Guo, J.H.; Zhai, M.G. Sm-Nd chronology of high-pressure sepiolite metamorphism in the Sanggan area of the North China Craton. *Chin. Sci. Bull.* **2000**, *45*, 2055–2061. [[CrossRef](#)]
79. Zhao, G.C.; Kröner, A.; Wilde, S.A.; Sun, M.; Li, S.Z.; Li, X.P.; Zhang, J.; Xia, X.P.; He, Y.H. Lithotectonic elements and geological events in the Hengshan-Wutai-Fuping belt: A synthesis and implications for the evolution of the Trans-North China Orogen. *Geol. Mag.* **2007**, *144*, 753–775. [[CrossRef](#)]
80. Zhang, J.; Zhao, G.C.; Li, S.Z.; Sun, M.; Wilde, S.A.; Liu, S.W.; Yin, C.Q. Polyphase deformation of the Fuping Complex, Trans-North China Orogen: Structures, SHRIMP U-Pb zircon ages and tectonic implications. *J. Struct. Geol.* **2009**, *31*, 177–193. [[CrossRef](#)]
81. Guo, J.H.; Zhai, M.G.; Li, Y.G.; Yan, Y.H. Contrasting metamorphic P-T paths of Archaean high-pressure granulites from the North China Craton: Metamorphism and tectonic significance. *Acta Petrol. Sin.* **1998**, *14*, 430–448, (In Chinese with English Abstract).
82. Guo, J.H.; Zhai, M.G. Sm-Nd age dating of high-pressure granulites and amphibolite from Sanggan area, North China craton. *Chin. Sci. Bull.* **2001**, *46*, 106–111. [[CrossRef](#)]
83. Liu, J.Z.; Zhang, F.Q.; Ouyang, Z.Y.; Li, C.L.; Xu, L. Geochemistry and chronology of the Jiehekou Group metamorphic basic volcanic rocks in the Lüliang Mountain area, Shanxi, China. *Sci. China (Ser. D)* **2003**, *46*, 1171–1181. [[CrossRef](#)]
84. Faure, M.; Trap, P.; Lin, W.; Monié, P.; Bruguier, O. Polyorogenic evolution of the Paleoproterozoic Trans-North China Belt: New insights from the Lüliangshan-Hengshan-Wutaishan and Fuping massifs. *Episodes* **2007**, *30*, 96–106. [[CrossRef](#)] [[PubMed](#)]
85. Kusky, T.M.; Windley, B.; Zhai, M.G. Tectonic evolution of the North China Block: From orogen to craton to orogen. *Geol. Soc. Lond. Spec. Publ.* **2007**, *280*, 1–34. [[CrossRef](#)]
86. Tracy, R.J. Compositional zoning and inclusions in metamorphic minerals. *Geo Sci. World* **1982**, *10*, 354–398.
87. Wang, Z.H.; Wilde, S.A.; Wan, J.L. Tectonic setting and significance of 2.3–2.1 Ga magmatic events in the Trans-North China Orogen: New constraints from the Yanmenguan mafic-ultramafic intrusion in the Hengshan-Wutai-Fuping area. *Precambrian Res.* **2010**, *178*, 27–42. [[CrossRef](#)]
88. Liu, S.W. Study of P-T pathway of hematite in Fuping area. *Geol. J. Univ.* **1996**, *1*, 75–84. (In Chinese)
89. Zhao, G.C.; Wilde, S.A.; Sun, M.; Guo, J.H.; Kröner, A.; Li, S.Z.; Li, X.P.; Zhang, J. SHRIMP U-Pb zircon geochronology of the Huai’an Complex: Constrains on Late Archean to Paleoproterozoic magmatic and metamorphic events in the Trans-North China Orogen. *Am. J. Sci.* **2008**, *308*, 270–303. [[CrossRef](#)]
90. Zhao, J.; Zhai, R.; Qian, Z.; Ma, R. A Study on Springback of Profile Plane Stretch-Bending in the Loading Method of Pretension and Moment. *Int. J. Mech. Sci.* **2013**, *75*, 45–54. [[CrossRef](#)]
91. Pattison, D.R.M.; Chacko, T.; Farquhar, J.; Mcfarane, C.R.M. Temperatures of granulite-facies metamorphism: Constraints from experimental phase equilibria and thermobarometry corrected for retrograde exchange. *J. Petrol.* **2003**, *44*, 867–900. [[CrossRef](#)]
92. Liu, D.Y.; Page, R.W.; Compston, W.; Wu, J.S. U-Pb zircon geochronology of late Archaean metamorphic rocks in the Taihangshan-Wutaishan area, North China. *Precambrian Res.* **1985**, *27*, 85–109. [[CrossRef](#)]
93. Zhai, M.G.; Santosh, M. The early Precambrian odyssey of the North China Craton: A synoptic overview. *Gondwana Res.* **2011**, *20*, 6–25. [[CrossRef](#)]
94. Liao, Y.; Wei, C. Ultrahigh-temperature mafic granulite in the Huai’an Complex, North China Craton: Evidence from phase equilibria modelling and amphibole thermometers. *Gondwana Res.* **2019**, *76*, 62–76. [[CrossRef](#)]

95. Indares, A.D. Metamorphic textures and P-T evolution of high-P granulites from the Lelukauu terrane, NE Grenville Province. *J. Metamorph. Geol.* **2003**, *21*, 35–48. [[CrossRef](#)]
96. Wilde, S.A.; Cawood, P.A.; Wang, K.Y.; Nemchin, A.; Zhao, G.C. Determining Precambrian crustal evolution in China: A case-study from Wutaishan, Shanxi Province, demonstrating the application of precise SHRIMP U-Pb geochronology. In *Aspects of the Tectonic Evolution of China*; Special Publications 226; Malpas, J., Fletcher, C.J.N., Ali, J.R., Aichison, J.C., Eds.; Geological Society: London, UK, 2004; pp. 5–26. [[CrossRef](#)]

Disclaimer/Publisher’s Note: The statements, opinions and data contained in all publications are solely those of the individual author(s) and contributor(s) and not of MDPI and/or the editor(s). MDPI and/or the editor(s) disclaim responsibility for any injury to people or property resulting from any ideas, methods, instructions or products referred to in the content.